

1    **Descriptions of four new species of**  
2    ***Minyomerus* Horn, 1876 sec. Jansen &**  
3    **Franz, 2018 (Coleoptera: Curculionidae),**  
4    **with notes on their distribution and**  
5    **phylogeny**

6    **M. Andrew Jansen<sup>1</sup> and Nico M. Franz<sup>2</sup>**

7    **<sup>1</sup>School of Life Sciences, 427 E Tyler Mall, PO Box 874501, Tempe, AZ 85287**

8    **<sup>2</sup>ASU Natural History Collections, 734 W Alameda Dr, Tempe, AZ 85282**

9    Corresponding author:

10    M. Andrew Jansen<sup>1</sup>

11    Email address: majanse1@asu.edu

12    **ABSTRACT**

13    This contribution adopts the taxonomic concept approach, including the use of *taxonomic concept labels*  
14    (name sec. [*according to* source] and Region Connection Calculus (RCC–5) articulations and alignments).  
15    Prior to this study, the broad-nosed weevil genus *Minyomerus* Horn, 1876 sec. Jansen & Franz, 2015  
16    (Curculionidae [non-focal]: Entiminae [non-focal]: Tanymecini [non-focal]) contained 17 species distributed  
17    throughout the desert and plains regions of North America. In this review of *Minyomerus* sec. Jansen &  
18    Franz, 2018, we describe the following four species as new to science: *Minyomerus ampullaceus* sec.  
19    Jansen & Franz, 2018 (henceforth: [JF2018]), **new species**, *Minyomerus franko* [JF2018], **new species**,  
20    *Minyomerus sculptilis* [JF2018], **new species**, and *Minyomerus tylotos* [JF2018], **new species**. The four  
21    new species are added to, and integrated with, the preceding revision, and an updated key and phylogeny  
22    of *Minyomerus* [JF2018] are presented. A cladistic analysis using 52 morphological characters of 26  
23    terminal taxa (5/21 outgroup/ingroup) yielded a single most-parsimonious cladogram (Length = 99 steps,  
24    Consistency Index = 60, Retention Index = 80). The analysis reaffirms the monophyly of *Minyomerus*  
25    [JF2018] with eight unreversed synapomorphies. The species-group placements, possible biogeographic  
26    origins, and natural history of the new species are discussed in detail.

27    **INTRODUCTION**

28    This phylogenetic [revision study](#) follows Jansen & Franz (2015) in the use of the taxonomic concept  
29    approach; see Franz & Peet (2009), Franz et al. (2016a,b). Accordingly:

- 30    1. *Taxonomic concept labels* – i.e., the taxonomic name sec. (*according to* author or source (year) –  
31    are used whenever we identify one specific usage of the taxonomic name. Examples: *Minyomerus*  
32    Horn, 1876 sec. Jansen & Franz, 2015 (henceforth: [JF2015]) and *Minyomerus* Horn, 1876  
33    sec. Jansen & Franz, 2018 (henceforth: [JF2018]). We also employ this convention to express  
34    nomenclatural relationships.
- 35    2. Solely the taxonomic name – without the sec. annotation – is used to refer to the cumulative  
36    history (origin to present) of taxonomic concept labels in which that name participates. Example:  
37    *Minyomerus* Horn, 1876.
- 38    3. The annotation [non-focal] is added to taxonomic names whose meanings are not under scrutiny in  
39    the present context; such as names for higher-level weevil groups and associated plants (exempting  
40    common names). Example: Tanymecini Lacordaire, 1863 [non-focal].

41    The weevil genus *Minyomerus* Horn, 1876 [JF2018] remains currently assigned to the tribe Tanymecini  
42    Lacordaire, 1863 [non-focal], subtribe Tanymecina Lacoirdaire, 1863 [non-focal] (Curculionidae [non-

43 focal]: Entiminae [non-focal] – higher-level classification in accordance with Alonso-Zarazaga & Lyal  
44 1999 and Bouchard et al. 2011). A recent phylogenetic revision of the genus *Minyomerus* [JF2015]  
45 recognized a total of 17 described species, distributed throughout the desert and plains regions of North  
46 America (Jansen & Franz 2015).

47 Members of the genus *Minyomerus* [JF2018] are phytophagous, and may be found on a variety of  
48 host plants, especially the creosote bush *Larrea tridentata* (DC) Coville [non-focal] (Zygophyllaceae  
49 [non-focal]), broomweed *Gutierrezia Lagasca* [non-focal] (Asteraceae [non-focal]), sagebrush *Artemisia*  
50 Linnaeus [non-focal] (Asteraceae [non-focal]), and occasionally on other various members of Asteraceae  
51 [non-focal] (Jansen & Franz 2015). While many species appear to be generalists, the adults are consis-  
52 tently observed on the leaves and branches of the host, feeding on the leaf tissue. All other life stages  
53 remain unknown. Species of *Minyomerus* [2018] are commonly found in deserts throughout western  
54 North America; including the Mojave, Sonoran, Chihuahuan, and Great Basin Deserts. However, their  
55 distributional range extends throughout the semi-arid regions of the Great Plains, the Colorado Plateau,  
56 and Baja California, México (O'Brien & Wibmer 1982, Jansen & Franz 2015). The adults are flightless,  
57 as the hind wings and associated flight structures of all species are either greatly reduced or not readily  
58 apparent in dissection.

59 *Minyomerus* [JF2018] belongs to the broad-nosed weevils, subfamily Entiminae [non-focal], on the  
60 basis of having a short, broad rostrum and dehiscent mandibular process (Marvaldi 1997, Anderson 2002,  
61 Oberprieler et al. 2007, 2014, Marvaldi et al. 2014). The adults are clothed in appressed, circular scales,  
62 generally in earth-tones from white to dark brown, with sub-recumbent to erect, interspersed setiform  
63 scales ("setae") arranged in rows on the elytral intervals. Their body length can range from 2.8 mm to 6.0  
64 mm (Jansen & Franz 2015). The genus has been classified in the tribe Tanymercini [non-focal] based on  
65 the presence of post-ocular vibrissae that project anteriorly from the anterior prothoracic margin, although  
66 the exact placement and sister taxa of this genus within the tribe are currently unknown (Howden 1959,  
67 1970, 1982, Jansen & Franz 2015).

68 *Minyomerus* [JF2015] was circumscribed by a unique combination of synapomorphic traits, described  
69 by Jansen & Franz (2015) as follows:

- 70 1. The integument is covered by appressed scales that are sub-circular and overlap posteriorly.
- 71 2. The nasal plate is present as a broad, scale-covered, chevron-shaped ridge demarcating the epistoma.
- 72 3. A sulcus posteriad of nasal plate is present.
- 73 4. The scrobe is sub-equal in length to the funicle and club combined.
- 74 5. The head is directed slightly ventrally.
- 75 6. The metatibial apex lacks setiform bristles yet displays bristles that are shorter to sub-equal in  
length to the surrounding setae and conical to lamelliform.
- 76 7. The mesotarsi are slightly shorter than the mesotibiae.
- 77 8. All tarsi lack pads of setiform setae but have stout, spiniform setae.

79 The following additional characters are useful for identifying members of *Minyomerus* [JF2018],  
80 especially when differentiating the former from other genera of Tanymercini [non-focal] that may be  
81 found together in the same desert habitats; viz. *Isodrusus* Sharp, 1911 [non-focal], *Isodacrys* Sharp, 1911  
82 [non-focal], and *Pandeleteinus* Champion, 1911 [non-focal] (see also Anderson 2002):

- 83 1. The intercoxal process of the prosternum is medially divided into two halves, with the procoxae  
84 apparently contiguous in most.
- 85 2. The elytral humeri are rounded rather than angled and protruding.
- 86 3. The profemora are not dilated and lack spines.
- 87 4. The protibiae are ventrally excavated by a longitudinal groove or concavity.
- 88 5. A distinct scrobe is present and directed ventrad of the eye, with a more or less apparent tooth  
formed by an overhang of the dorsal margin.

90 Following the publication of a monographic revision of *Minyomerus* [JF2015], we have discovered  
91 four additional, undescribed species. These are known to us only from limited numbers of specimens, yet  
92 are well circumscribed by – i.e., intensionally included in (see Franz & Peet 2009) – the recent generic  
93 delimitation of *Minyomerus* [JF2015]. In other words, the addition of these new species *has not* required  
94 altering the intensional, property-based definition of the genus-level concept as circumscribed in Jansen

& Franz (2015) (see **Phylogenetic Results**). Our RCC–5 alignments (see **RCC–5 Alignments**) reflect this genus-level concept congruence while also showing which classificatory and phylogenetic structures have changed (Figs. 32–34). The precise use of the taxonomic concept labels in accordance with either [JF2015] or [JF2018] is meant to minimize the creation of new taxonomic concept labels (to counter label “inflation”; see Franz & Peet (2009)), while reflecting explicitly *which* taxonomic concepts we consider as relevantly new and unique to the present study.

Here we describe the four newly found species of *Minyomerus* [JF2018] and provide images of the holotypes and of dissected genitalia for the purpose of identification. We additionally conduct a morphological phylogenetic analysis of the genus to clarify the placement of these new taxa within *Minyomerus* [JF2018], based on the analysis provided in our previous work. An emended identification key to the species of *Minyomerus* [JF2018] is given, along with an updated species checklist. Where possible, we make note of host-plant records, and briefly discuss the geographic distributions of the herein described species. A more extensive discussion of the habits, distribution, and delimitation of the genus *Minyomerus* [JF2015] and all of its constituent species is provided in Jansen & Franz (2015).

## 109 MATERIALS AND METHODS

110 The methods used in this manuscript are generally consistent with Jansen & Franz (2015). Relevant  
111 updates are detailed below. In particular, we retain the format for the species descriptions, emphasizing  
112 only those characters that vary significantly from the generic circumscription of *Minyomerus* [JF2015].

### 113 Acquisition of museum specimens

114 The set of specimens used in Jansen & Franz (2015) was supplemented with material from the following  
115 collections, using the codens of Arnett Jr. et al. (1993):

116 **CMNC** Canadian Museum of Nature Collection, Ottawa, Ontario, Canada

117 **TAMU** Texas A & M University, College Station, Texas, USA

118 **USNM** National Museum of Natural History, Washington, D.C., USA

119 Georeferencing of localities was performed with Google Earth (Google Inc. 2018), following the  
120 WGS 84 standard, and reported in decimal degrees. Taxonomic names for associated host plants, as noted  
121 following each species account, are used in accordance with Munz & Keck (1973) and SEINet (2018).

### 122 Morphological analysis

123 Our systematic and descriptive approach is complementary to Jansen & Franz (2015), which in turn  
124 follows Franz (2010a,b, 2012). The terminology for exterior morphology is in general accordance  
125 with de la Torre-Bueno et al. (1989). Additional morphological terms specific to broad-nosed weevils  
126 (Entiminae [non-focal]) were used as follows: Ting (1936) and Morimoto & Kojima (2003) for mouthparts;  
127 Thompson (1992) for tibial apices and abdominal segments; and Oberprieler et al. (2014) and Howden  
128 (1995) for male and female terminalia.

129 Measurements were taken with a Leica M205 C stereomicroscope and associated software, Leica  
130 Application Suite (LAS), version 4.1.0. Overall body length and width were measured in dorsal view  
131 as the maximum distance between the rostral and elytral apices, and the maximum width of both elytra,  
132 respectively. Rostral length was measured in dorsal view as the distance between the epistomal apex and  
133 the anterior margin of the eyes. Rostral width was measured in dorsal view as the maximum distance  
134 between the dorsal margins of the rostrum near the point of antennal insertion. Pronotal length was  
135 measured in dorsal view as the length along the midline between the anterior and posterior margins.  
136 The width of an individual elytron was measured in dorsal view as the maximum distance between the  
137 lateral margin and the elytral suture. Other length and width measurements were also performed in dorsal  
138 orientation, using the maximum length and width of the corresponding structure (profemur, protibia,  
139 elytron, and aedeagus). Images of mouthparts and terminalia were produced with the Leica microscope  
140 equipment, while habitus photographs were created with a Visionary Digital Passport II system using a  
141 Canon EOS Mark 5D II camera.

142 The herein newly recognized species of *Minyomerus* [JF2018] were delimited through application  
143 of the phylogenetic species concept *sensu* Wheeler & Platnick (2000). Species descriptions are in  
144 alphabetical order, rather than phylogenetic order, for ease of use. As in Jansen & Franz (2015), the

145 species descriptions represent unique, complementary accounts of the character states observed for each  
 146 species, including their intra-specific variability, but excepting characters invariant within the genus-level  
 147 concept of *Minyomerus* [JF2015]. Likewise, descriptions of males emphasize characters that are variable  
 148 and sufficiently different from those of the females to merit recognition. The key to identifying species of  
 149 *Minyomerus* [JF2018] is arranged with emphasis being placed on the most readily observable diagnostic  
 150 characters. This manuscript is arranged with the species descriptions appearing first, followed by the key  
 151 to species, and then by the phylogenetic and RCC–5 alignment results.

## 152 Phylogenetic analysis

153 The morphological cladistic analysis includes 26 terminal taxa; with 21 ingroup and 5 outgroup terminals.  
 154 The ingroup terminals were represented by 17 species previously assigned to *Minyomerus* [JF2015]  
 155 and four newly recognized species. In keeping with our previous analysis, we sampled outgroups fairly  
 156 broadly while remaining focused on North American lineages that are putative close relatives of the  
 157 ingroup (Jansen & Franz 2015, Nixon & Carpenter 1993).

158 Although the tribe Tanytacra [non-focal] is cosmopolitan, the majority of New World species  
 159 diversity in the tribe may be found in the subtribe Tanytacrina [non-focal] (Alonso-Zarazaga & Lyal  
 160 1999). Thus, four of the five outgroup terminals are represented by species belonging to separate genera  
 161 in the Tanytacrina [non-focal]; viz. *Isodacrys buchanani* Howden, 1961 [non-focal], *Isodrusus debilis*  
 162 Sharp, 1911 [non-focal], *Pandeleteinus subcancer* Howden, 1969 [non-focal], and *Pandeleteius cinereus*  
 163 (Horn, 1876) [non-focal]. Because generic relationships in the Tanytacra [non-focal] remain unresolved,  
 164 we selected a relatively far-removed taxon to root the cladogram that would nevertheless display states  
 165 applicable to the ingroup for characters under consideration (Rieppel 2007, Franz 2014). To this end we  
 166 used the North American species *Sitona californicus* (Fahraeus, 1840) [non-focal], of the tribe Sitonini  
 167 Gistel, 1856 [non-focal].

168 The character matrix was edited and phylogenetic results viewed using the WinDada and WinClados  
 169 interfaces of WinClada, respectively (Nixon et al. 2002). ~~The character sequence follows that of the~~  
 170 ~~taxonomic descriptions. Characters are numbered in accordance with descriptive sequence used in the~~  
 171 ~~species accounts. A “–” symbol indicates inapplicable (character, state), whereas a “?” symbol indicates~~  
 172 ~~missing information, e.g., due to the unavailability of male specimens or insufficient specimens on hand~~  
 173 ~~to permit full dissections. Characters 9, 27, 39, 45 - 47, 49, and 51 were mapped onto the preferred~~  
 174 ~~phylogeny using ACCTRAN optimization (see Agnarsson & Miller 2008), and the remaining characters~~  
 175 ~~had an unambiguous optimization. All multi-state characters but one were coded as additive, as explained~~  
 176 ~~beneath the description for each character (see Phylogenetic Results), based on their alignment with the~~  
 177 ~~preferred phylogeny. Each alternative coding scheme was tested both alone and in unison with the other~~  
 178 ~~multi-state characters to assess their impact on the topology of the preferred phylogeny.~~

179 The most parsimonious tree and character state optimizations were inferred under parsimony using  
 180 NONA (Goloboff 1999). An unconstrained heuristic search was conducted using the commands: hold  
 181 100001, mult\*1000, hold/100, with mult\*max\* selected. Bootstrap support was inferred in  
 182 WinClada using the parameters of 1000 replications, hold 1000, hold/100, mult\*10,  
 183 Don't do max\*, and Save consensus. Finally, Bremer support values (Bremer et al. 1994) and  
 184 relative fit difference (Goloboff & Farris 2001) were calculated in NONA using the commands: hold  
 185 1001, sub 20, bs for Bremer support values, and bs\* for relative fit difference, respectively (Goloboff  
 186 et al. 2008).

187 The motivation for providing Bremer support values and relative fit difference comes from their  
 188 respective interpretations, based on how the measures are calculated, *per* Goloboff & Farris (2001).  
 189 Both of these indices rely on summation of the number of favorable and contradictory characters when  
 190 comparing a most-parsimonious tree to a suboptimal tree. If the step length of the  $i^{\text{th}}$  character ( $I$ ) of  
 191  $n$  total characters on the most-parsimonious tree ( $L_{MPT}$ ) is less than its corresponding step length on  
 192 the suboptimal tree ( $L_{SUB}$ ), the character is designated as favorable ( $f_i$ ), but if the opposite is true, the  
 193 character is designated as contradictory ( $c_i$ ), and expressed formally:

$$I = \begin{cases} f_i & L_{MPT} < L_{SUB} \\ c_i & L_{MPT} > L_{SUB} \end{cases} \quad (1)$$

Where the number of favorable ( $F$ ) and contradictory ( $C$ ) characters are defined, respectively, as:

$$F = \sum_{n=0}^i f_i \quad (2)$$

$$C = \sum_{n=0}^i c_i \quad (3)$$

Bremer support values (bsv) and relative fit difference (rfd) are then calculated simply as:

$$\text{bsv} = F - C \quad (4)$$

$$\text{rfd} = \frac{F - C}{F} \times 100 \quad (5)$$

The Bremer support value for a node thus indicates how many more characters support a node than contradict it, while the relative fit difference indicates what proportion of the favorable characters are represented by the Bremer support value. Whereas the Bremer support value is as large as the number of characters supporting the node, in excess of the contradicting characters, the relative fit difference can only vary from 0 to 100, as a proportion of the number of supporting characters. By providing both measures, one may quickly discriminate, for example, between a node supported by 4 characters but contradicted by 1 character (bsv = 3, rfd = 75), and a node supported by 10 characters but contradicted by 7 characters (bsv = 3, rfd = 30).

### Taxonomic annotations and RCC–5

In accordance with Jansen & Franz (2015), we use the symbol “=” to indicate nomenclatural synonymy (objective/subjective); and the RCC–5 symbols {==, >, <, ><, !} indicate taxonomic concept articulations. The annotations (INT) and (OST) indicate intensional and ostensive readings of articulations, and AND is used to connect multiple simultaneously recognized provenance relationships. Two *intensional* alignments are produced as part of this [revisionreview](#), i.e., one that captures the non-/congruence of *Minyomerus* [JF2018] versus *Minyomerus* [JF2015] represented as rank-only classifications (Fig. 32), and another that represents these as fully bifurcated phylogenies with newly assigned clade concept labels, shown in whole-concept resolution (Fig. 33) and in split-concept resolution (Fig. 34); see Franz et al. (2018).

A detailed breakdown of our alignment approach and outcomes using an RCC–5 logic reasoner toolkit (Chen et al. 2014) is provided in the **Supplemental Information, S11 to S14**. For further information, see also Jansen & Franz (2015), Franz et al. (2016a,b).

### Species distribution modeling

We used the modeling program Maxent, Version 3.4, to generate habitat models for the species of *Minyomerus* [Minyomerus](#) [JF2018] (Figs. 35–38) based on documented occurrence records (Phillips et al. 2004, 2006, Elith et al. 2011). The default settings were adjusted to Max number background points = 100,000 and Iterations = 10. Cross-validation was used to leverage all available locality data; however, no models could be created for species with two or fewer documented localities. We selected 19 bioclimatic variables and elevation as Environmental Layers in Maxent, obtained from WorldClim (Hijmans et al. 2005). The layers were downloaded by tile (zones 11–13 and 21–23), with a 30 arc-second resolution (projected using WSG 84) to provide adequate coverage of the full distribution of the genus. Layerwise assembly of tiles was done using QGIS, Version 2.18.16 ‘Las Palmas’, creating composite maps of six tiles each to use in species distribution modeling (Quantum GIS Development Team 2018).

The rasterized predictive probabilities were imported into QGIS, where each file was designated a specific color. Each pixel in the raster was assigned a linearly interpolated saturation of that color, with increasing saturation denoting an increased probability of successful prediction of species presence at that point. Pixels with a value below 0.50 were rendered transparent so that the maps only show regions with a greater than 50% chance of successful prediction. The raster files were clipped to remove extraneous predicted regions based on: (1) predictive probability (i.e., removing large areas with only transparent pixels) and (2) geographic extent (accounting for endemicity). For example, a species endemic to the Snake River Valley of Idaho does not require a predictive model for bioclimatically similar habitats in the

228 Chihuahuan Desert. Documented occurrence records are laid over the modeled habitat ranges as colored  
229 circles on their respective maps (Figs. 36-38), along with vector layers of country (white) and state (gray)  
230 borders (Hijmans et al. 2012).

231 **Nomenclature**

232 The electronic version of this article in Portable Document Format (PDF) will represent a published work  
233 according to the International Commission on Zoological Nomenclature (ICZN), and hence the new names  
234 contained in the electronic version are effectively published under that Code from the electronic edition  
235 alone. This published work and the nomenclatural acts it contains have been registered in ZooBank, the  
236 online registration system for the ICZN. The ZooBank LSIDs (Life Science Identifiers) can be resolved  
237 and the associated information viewed through any standard web browser by appending the LSID to  
238 the prefix <http://zoobank.org/>. The LSID for this publication is: urn:lsid:zoobank.org:pub:0AEE5733-  
239 06D1-401F-88C9-0D5232FBFC7A. The online version of this work is archived and available from the  
240 following digital repositories: PeerJ, PubMed Central and CLOCKSS.

241 *Minyomerus ampullaceus*: *Minyomerus franko*: *Minyomerus sculptilis*: *Minyomerus tylotos*:

242 **DESCRIPTIONS OF NEW SPECIES**

243 ***Minyomerus ampullaceus* Jansen & Franz sec. Jansen & Franz, 2018; sp. n.**

244 urn:lsid:zoobank.org:act:24943E17-F20E-4E3C-A3A1-A1D4D907B48E

245 Figures 1-6

246 **Diagnosis**

247 *Minyomerus ampullaceus* [JF2018] is best differentiated from other congeners by its unique body shape,  
248 which most prominently features a strongly constricted, sub-cylindrical pronotum and greatly protuberant  
249 elytra; this combination gives the species a distinctly flask- or bottle-shaped appearance. Due to the  
250 relatively poor condition of the scales and setae of the holotype, color and setation cannot be reliably  
251 used for identification. However, the elytra themselves are unique in shape, and diagnostic, together  
252 nearly 2× the width of the pronotum at their widest point, and nearly 3/4× as wide as long in dorsal  
253 view. In lateral view the anterior and posterior declivities of the elytra are strongly abrupt, and nearly  
254 vertical; most notably, the anterior margin of the elytra projects strongly and characteristically dorsad of  
255 its articulation with the posterior pronotal margin. The spermatheca is also quite distinct, having a highly  
256 elongate projection of the corpus aligned with midline of the ramus, which is basally tapered and angled  
257 at nearly 45° to the corpus.

258 **Description of female**

259 **Habitus** Length 3.76 mm, width 1.76 mm, length/width ratio 2.14, widest at anterior 1/3 of elytra.  
260 Integument orange-brown to black. Scales with variously interspersed colors ranging from slightly  
261 off-white to beige to yellow. Setae recumbent to sub-recumbent, white to brown in color.

262 **Mandibles** Partially covered with white, slightly opalescent scales, with 3 longer setae, and 1 shorter  
263 seta between these.

264 **Rostrum** Length 0.54 mm, anterior portion 1.5-2× broader than long, rostrum/pronotum length ratio  
265 0.57, rostrum length/width ratio 1.10. Separation of rostrum from head generally obscure. Dorsal outline  
266 of rostrum nearly square, anterior half of dorsal surface mesally concave, posterior half coarsely but  
267 shallowly punctate to rugose. Rostrum in lateral view nearly square; apical margin broadly bisinuate and  
268 emarginate, with 2 pairs of large vibrissae. Nasal plate defined by Y-shaped, impressed lines, convex,  
269 integument partially covered with white scales. Margins of mandibular incision directed ca. 15° outward  
270 dorsally in frontal view. Ventrolateral sulci strongly defined, beginning as a narrow sulcus posteriad of  
271 insertion point of mandibles, running parallel to scrobe, terminating in a ventral fovea.

272 **Antennae** Small tooth formed by overhanging dorsal margin of scrobe directly ventrad of margin of  
273 eye. Scape extending to posterior 1/3 of eye. Funicular segments V-VII and club missing.

274 **Head** Eyes globular, anterodorsal margin of each eye feebly impressed, posterior margin elevated  
275 from lateral surface of head; eyes separated in dorsal view by 4× their anterior-posterior length, set off  
276 from anterior prothoracic margin by 1/3 of their anterior-posterior length. Head without any transverse  
277 post-ocular impression.

278 **Pronotum** Length/width ratio 0.88; widest near midpoint. Anterior margin slightly arcuate, lateral  
279 margins curved and widening into a bulge just anteriad of midpoint of pronotum, posterior margin straight,  
280 with a slight mesal incurvature. Pronotum in lateral view with setae that reach beyond anterior margin by  
281 1/2 of their length; these setae becoming evenly longer and more erect laterally, reaching a maximum  
282 length equal to 1/2 of length of eye. Anterolateral margin with a reduced tuft of 6-7 post-ocular vibrissae  
283 present, emerging near ventral 1/2 of eye, and stopping just below ventral margin of eye; vibrissae sub-  
284 equal in length at 1/3 of anterior-posterior length of eye, except for three vibrissae achieving a maximum  
285 length similar to anterior-posterior length of eye.

286 **Scutellum** Exposed, margins straight.

287 **Pleurites** Metepisternum hidden by elytron.

288 **Thoracic sterna** Mesocoxal cavities separated by 1/4× width of mesocoxal cavity. Metasternum with  
289 transverse sulcus not apparent; metacoxal cavities widely separated by ca. 2× their width.

290 **Legs** Profemur/pronotum length ratio 1.04; profemur with distal 1/5 produced ventrally as a rounded  
291 projection covering tibial joint; condyle of tibial articulation occupying 4/5 of distal surface and 1/5  
292 length of femur. Protibia/profemur length ratio 0.93; protibial apex with ventral setal comb recessed in  
293 an incurved groove; mucro present as a large, black, sub-triangular, medially-projected tooth, which is  
294 approximately equilateral and whose sides are sub-equal in length to surrounding setae. Protarsus with  
295 tarsomere III 1.25× as long as II; wider than long. Metatibial apex with almond shaped convexity ringed  
296 by 10 short, spiniform setae.

297 **Elytra** Length/width ratio 2.66; widest at anterior 1/3; anterior margins jointly almost 2× wider than  
298 posterior margin of pronotum and strongly produced dorsally from margin of pronotum; lateral margins  
299 evenly rounded until posterior 1/3, more strongly rounded and converging thereafter. Posterior declivity  
300 angled at nearly 85° to main body axis. Elytra with 10 complete striae; striae shallow; punctures faint  
301 beneath appressed scales, separated by 5-7× their diameter; intervals very slightly elevated.

302 **Abdominal sterna** Ventrite III anteromesally incurved around a fovea located mesally on anterior  
303 margin, posterior margin elevated and set off from IV along lateral 1/3s of its length. Sternum VII mesally  
304 1/2× as long as wide; anterior margin weakly curved.

305 **Tergum** Pygidium (tergum VIII) sub-conical; posterior margin emarginate; medial 1/3 of anterior 3/5  
306 of pygidium less sclerotized.

307 **Sternum VIII** Anterior laminar edges each incurved forming a 115° angle with lateral margin, this angle  
308 distinctly sclerotized; posterior 1/2 of lamina porose throughout, laminar arms more sclerotized medially;  
309 posterior edge evenly, moderately arcuate.

310 **Ovipositor** Coxites in dorsal view slightly longer than broad, with a medial region that is weakly  
311 sclerotized.

312 **Spermatheca** Comma-shaped; collum expanded to form a long, cylindrical projection, sub-equal in  
313 length to ramus, 1/3× width of corpus, angled at 45° to corpus, apically with a reduced hood-shaped  
314 projection; ramus elongate, bulbous, slightly wider than thickness of corpus, basally constricted to form a  
315 short stalk; corpus not greatly swollen; cornu sub-equal in length to corpus and collum, recurved distally  
316 to form an inner angle of 60° to corpus, straight and gradually narrowing along basal 2/3, with apical 1/3  
317 abruptly narrowed, angled at 45° to corpus, and tapering to a slight knob.

318 **Description of male**

319 Male not available or known.

320 **Comments**

321 Due to the limited number of specimens of this species, dissections of mouthparts could not be performed.

322 **Etymology**

323 Named in reference to the shape of the body in dorsal view, which appears bottle-shaped due to the large  
324 elytra and comparatively cylindrical pronotum – *ampullaceus* = "flasklike"; Latin adjective (Brown 1956).

325 **Material examined**

326 **Holotype** ♀ “Carlsbad, N.M.; Geococcyx calif; 144640” (USNM).

327 **Distribution**

328 This species is known only from Carlsbad, New Mexico (USA), from an unspecified locality; the location  
329 of the city is shown in Fig. 36.

330 **Natural history**

331 No host plant associations have been documented. The label indicates “Geococcyx calif”; this is pre-  
332 sumably a reference to *Geococcyx californianus* (Lesson, 1829) [non-focal] (Cuculidae [non-focal]),  
333 the Greater Roadrunner, ~~although it is unclear if the specimen was found on or near one of these birds~~  
334 ~~(either living, dead, or in a nest). Species of Minyomerus JF2018 are only known to be phytophagous,~~  
335 ~~not parasitic, phoretic, or necrophagous. Hence we believe that this~~. We had initially believed that  
336 ~~this indicated a specimen found in a roadrunner nest; however, according to our reviewers, the USNM~~  
337 ~~frequently assisted with the identification of insect specimens retrieved from the stomach contents of~~  
338 ~~birds, and thus the specimen was most likely found in a nest, and was present there only incidentally~~  
339 ~~because the nest was constructed in the host plant of this specimen (Jansen & Franz 2015) retrieved from~~  
340 ~~the gut contents of a roadrunner. This seems quite likely given the poor external condition of the~~  
341 ~~specimen.~~ It is unknown whether this species is parthenogenetic.

342 **Minyomerus franko Jansen & Franz sec. Jansen & Franz, 2018; sp. n.**

343 urn:lsid:zoobank.org:act:F8C0153E-DF0E-40E0-AF31-EBEA7075D06D

344 Figures 7-15

345 **Diagnosis**

346 *Minyomerus franko* [JF2018] is readily distinguished from other congeners by the strikingly long setae  
347 of the anterior margin of the pronotum, which project laterally up to 80° from the longitudinal axis of  
348 the body and achieve a maximum length at least equaling the diameter of the eye. In addition, the setae  
349 lining the dorsal margin of the ocular impression are elongate and reach a length equal to 1/2 - 3/4 × the  
350 diameter of the eye. The spermatheca has a short, somewhat bulbous corpus, with the ramus sub-equal  
351 in size and perpendicular to the corpus, and the collum is strongly recurved along the basal 1/3 of its  
352 length. The aedeagus is relatively short and wide, and is abruptly constricted in the apical 1/5 of its length,  
353 thereafter tapered to a rounded point.

354 **Description of female**

355 **Habitus** Length 3.10-3.30 mm, width 1.38-1.44 mm, length/width ratio 2.25-2.29, widest at anterior  
356 1/3-1/4 of elytra. Integument orange-brown to black. Scales with variously interspersed colors ranging  
357 from slightly off-white or beige to manila/tan to dark coffee brown, in some specimens appearing semi-  
358 translucent (in others opaque). Setae linear to slightly apically explanate, appearing minutely spatulate,  
359 sub-recumbent to sub-erect, white or brown in color.

360 **Mandibles** Covered with white scales, with 3 longer setae, and 1-2 shorter setae between these.

361 **Maxillae** Cardo bifurcate at base with an inner angle typically between 90–120°, arms of equal length,  
362 inner (mesal) arm nearly 1.5 × thicker than outer arm, both arms of bifurcation equal in length to apically  
363 outcurved arm, glabrous. Stipes sub-quadrata, roughly equal in length to each bifurcation of cardo, with a  
364 single lateral seta. Galeo-lacinial complex nearly extending to apex of maxillary palpomere II; complex  
365 mesally membranous, laterally sclerotized, with sharp demarcation of sclerotized region separating  
366 palpiger from galeo-lacinial complex; setose in membranous area just adjacent to sclerotized region, setae  
367 covering 2/3 of dorsal surface area; dorsally with 7 apicomosal lacinial teeth; ventrally with 4 reduced  
368 lacinial teeth. Palpiger with a single lateral seta, otherwise glabrous and evenly sclerotized throughout.

369 **Maxillary palps** I apically oblique, apical end forming a 45° angle with base, with 2 apical setae; II  
370 sub-cylindrical, with 1 apical seta.

371 **Labium** Prementum roughly trapezoidal; apical margins angulate, ventral margin gently sinuate, dorsal  
372 margin straight; lateral margins feebly incurved near posterior margin; basal margin arcuate. Labial palps  
373 3-segmented, I with apical 2/3 projecting beyond margin of prementum, exceeding apex of ligula; III  
374 slightly longer than II.

375   **Rostrum** Length 0.46-0.48 mm, anterior portion 1.75-2.25× broader than long, rostrum/pronotum  
376 length ratio 0.58-0.59, rostrum length/width ratio 1.21-1.26. Separation of rostrum from head generally  
377 obscure. Dorsal outline of rostrum sub-rectangular, anterior half of dorsal surface feebly impressed,  
378 posterior half coarsely but shallowly punctate to rugose. Rostrum in lateral view nearly square; apical  
379 margin bisinuate and emarginate, with 2 large vibrissae. Nasal plate defined by broad, V-shaped, shallowly  
380 impressed lines, anteromesally slightly convex, integument partially covered with white scales. Margins  
381 of mandibular incision directed ca. 15° outward dorsally in frontal view. Ventrolateral sulci weakly  
382 defined (or entirely absent in some specimens) as a broad concavity dorsad of insertion point of mandibles,  
383 running parallel to scrobe, becoming flatter posteriorly and disappearing ventrally. Dorsal surface of  
384 rostrum with short, linear, median fovea. Rostrum ventrally lacking sulci at corners of oral cavity.

385   **Antennae** Small tooth formed by overhanging dorsal margin of scrobe anterior to margin of eye by 1/5  
386 of length of eye. Scape nearly extending to posterior 1/4 of eye. Terminal funicular antennomere lacking  
387 appressed scales, having instead a covering of apically-directed pubescence with interspersed sub-erect  
388 setae. Club nearly 3× as long as wide.

389   **Head** Eyes globular to slightly elongate, slanted ca. 35° antero-ventrally; eyes separated in dorsal  
390 view by 4× their anterior-posterior length, set off from anterior prothoracic margin by 1/3 of their  
391 anterior-posterior length. Head without any transverse post-ocular impression.

392   **Pronotum** Length/width ratio 0.84-0.86; widest near anterior 1/3, between anterior constriction and  
393 midpoint. Anterior margin arcuate, lateral margins curved and widening into a slight bulge just anteriad  
394 of midpoint of pronotum, posterior margin straight, with a slight mesal incurvature. Pronotum in lateral  
395 view with setae that reach just beyond anterior margin, angled laterally at 45-80° to longitudinal axis, and  
396 strikingly long; these setae becoming evenly longer and more angled laterally, reaching a maximum length  
397 nearly equal to length of eye. Anterolateral margin with a reduced tuft of 5 post-ocular vibrissae present,  
398 emerging near ventral 1/2 of eye, and stopping just below ventral margin of eye; vibrissae sub-equal  
399 in length at 1/3× anterior-posterior length of eye, except for one vibrissa achieving a maximum length  
400 similar to anterior-posterior length of eye.

401   **Scutellum** Narrowly exposed, with visible area approximately equal to length of appressed scales,  
402 margins straight.

403   **Pleurites** Metepisternum nearly hidden by elytron except for triangular extension.

404   **Thoracic sterna** Mesocoxal cavities separated by 1/3× width of mesocoxal cavity. Metasternum with  
405 transverse sulcus not apparent; metacoxal cavities widely separated by ca. 2× their width.

406   **Legs** Profemur/pronotum length ratio 1.01-1.02; profemur with distal 1/5 produced ventrally as a sub-  
407 rectangular projection covering tibial joint; condyle of tibial articulation occupying 4/5 of distal surface  
408 and 1/5 length of femur. Protibia/profemur length ratio 0.86-0.89; protibial apex with ventral setal comb  
409 recessed in a subtly incurved groove; mucro present as a large, black, sub-triangular, medially-projected  
410 tooth, which is approximately equilateral and whose sides are sub-equal in length to surrounding setae.  
411 Protarsus with tarsomere III 2× as long as II; wider than long. Metatibial apex with almond shaped  
412 convexity ringed by 8-9 short, spiniform setae.

413   **Elytra** Length/width ratio 3.08-3.20; widest at anterior 1/3-1/4; anterior margins jointly 1.5× wider than  
414 posterior margin of pronotum; lateral margins sub-parallel to slightly rounded after anterior 1/3, more  
415 strongly rounded and converging in posterior 1/3. Posterior declivity angled at 70-85° to main body axis.  
416 Elytra with 10 complete striae; striae shallow; punctures faint beneath appressed scales, separated by  
417 5-7× their diameter; intervals very slightly elevated.

418   **Abdominal sterna** Ventrite III anteromesally incurved around a fovea located mesally on anterior  
419 margin, posterior margin elevated and set off from IV along lateral 1/3s of its length. Sternum VII mesally  
420 1/2× as long as wide; setae darkening, lengthening, and becoming more erect in posterior 2/3; anterior  
421 margin weakly curved.

422   **Tergum** Pygidium (tergum VIII) sub-cylindrical; medial 1/3 of anterior 2/3 of pygidium less sclerotized.

423   **Sternum VIII** Anterior laminar edges each incurved forming a 140° angle with lateral margin; slightly  
424 less sclerotized medially between arms of bifurcation; posterior edge subtly incurved medially.

425 **Ovipositor** Coxites 1.5× as long as broad, glabrous; styli 1/2× as long as coxites. Genital chamber  
426 apically sclerotized.

427 **Spermatheca** Comma-shaped; column short, apically with a large, hood-shaped projection angled  
428 at ca. 60° to ramus, nearly equal in length and contiously aligned with curvature of bulb of ramus;  
429 column sub-contiguous with, and angled at 90° to ramus; ramus elongate, sub-cylindrical to slightly  
430 bulbous, 4/5× thickness of corpus; corpus swollen, 1.25× thicknes of ramus and 1.5× thickness of cornu;  
431 cornu elongate, strongly recurved in basal 1/3, nearly straight thereafter and narrowing apically, abruptly  
432 narrowed in apical 1/3 with apex angled at 30° to corpus.

433 **Description of male**

434 Similar to female, except where noted.

435 **Habitus** Length 2.47-2.81 mm, width 0.99-1.24 mm, length/width ratio 2.27-2.49. Rostrum length  
436 0.30-0.42 mm, rostrum/pronotum length ratio 0.44-0.53, rostrum length/width ratio 1.00-1.08. Pronotum  
437 length/width ratio 0.91-1.00. Profemur/pronotum length ratio 0.87-0.90, protibia/profemur length ratio  
438 0.87-0.97. Elytra length/width ratio 3.00-3.10.

439 **Elytra** Elytral declivity more angulate than female on average, forming an 80° angle to main body axis,  
440 but otherwise as in female.

441 **Abdominal sterna** S sternum VII 2/5-1/2× as long as wide, posterior margin arcuate mesally.

442 **Tergum** Pygidium (tergum VIII) with posterior 1/3 punctate; anterior 2/3 rugose.

443 **Sternum IX** Spiculum gastrale 2× length of aedeagal pedon. Laminar alae located on lateral 1/4 of  
444 posterior margin.

445 **Aedeagus** Length/width ratio 2.78-3.16; lateral margins very slightly converging posteriorly, abruptly  
446 constricted and more strongly converging in apical 1/5. Pedon in lateral view becoming gradually narrower  
447 posteriorly in anterior 1/2, ventral margins in posterior 1/2 abruptly curving to meet dorsal margins at a  
448 rounded apical point. Flagellum with large, elonage, tortuous apical sclerite, sclerite nearly as long as  
449 pedon, with complex, asymmetrical interior structure.

450 **Etymology**

451 Named in reference to the long, somewhat unkempt, erect setae on the anterior margin of the pronotum—  
452 *franko* = "free"; Old High-German adjective (Brown 1956).

453 **Material examined**

454 **Holotype** ♀ "MEX: S.L.P 1 km N.; Entronque El Huizache; 1493 m 2.VI.87; R. Anderson, *Sphaeralcea*;  
455 *hastula* A. Gray" [non-focal] (**CMNC**).

456 **Paratypes** Same label information as female holotype (**CMNC**: 1 ♀, 1 ♂; **TAMU**: 2 ♂); "MEXICO:  
457 S.L.P; 19.6 mi. n. Huizache; July 25, 1976; Peigler, Gruetzmacher, R&M Murray, Schaffner" (**CMNC**: 1  
458 ♂); "MEXICO: San Luis Potosí; Entronque el Hulzache; 2 June 1987; R. Turnbow" (**CMNCUSNM**: 1 ♀;—  
459 **CMNC**: 1 ♂); "MEXICO: Tamaulipas; 8.8 mi. ne. Jaumave; October 10, 1973; Gaumer & Clark" (**TAMU**:  
460 2♀); "9 mi east Santo Domingo, S.L.P.; Mexico XI-14-68; Veryl V. Board" (**TAMU**: 2 ♂).

461 **Distribution**

462 This species has been found in San Luis Potosí and Tamaulipas (Mexico). It is likely to be found  
463 throughout the Chihuahuan Desert and arid regions of south-central Mexico based on habitat similarity  
464 (Fig. 37).

465 **Natural history**

466 Associated with spear globemallow *Sphaeralcea hastulata* A. Gray [non-focal] (Malvaceae [non-focal]).  
467 The indication of "Sphaeralcea hastula A. Gray" is not a valid name and appears to be a misspelling of  
468 *Sphaeralcea hastulata*.

469 **Minyomerus sculptilis Jansen & Franz sec. Jansen & Franz, 2018; sp. n.**

470 urn:lsid:zoobank.org:act:EA0B1AD9-68F2-4409-A0F8-903B0DA0FFF9

471 Figures 16-22

472 **Diagnosis**

473 *Minyomerus sculptilis* [JF2018] is best distinguished from other congeners, especially *Minyomerus*  
474 *imberbus* Jansen & Franz, 2015 [JF2015], by a combination of characters, as follows. The interspersed  
475 setae on the body are linear and either brown or white. The anterior margin of the pronotum bears a  
476 reduced tuft of post-ocular vibrissae. The head is barely elevated between the eyes. The ventrolateral  
477 sulci of the rostrum are well defined. The lateral face of each elytron has the intervals raised and well  
478 sculpted in appearance. The spermatheca is distinct and has an elongate, annulate, basally tapered ramus,  
479 which is slightly thinner than corpus. The cornu is strongly recurved in the basal half, giving it a uniquely  
480 sinuate appearance. Both the corpus and cornu terminate in large, hood-shaped, explanate projections  
481 equal in size to the ramus. The aedeagus is elongate, acutely angulate, and narrowing towards the apex  
482 more strongly in the region of the ostium.

483 **Description of female**

484 **Habitus** Length 3.39-3.70 mm, width 1.33-1.58 mm, length/width ratio 2.34-2.55, widest at anterior  
485 1/5 of elytra. Integument orange-brown to black. Scales with variously interspersed colors ranging from  
486 slightly off-white or beige to golden brown to dark coffee brown. Setae sub-recumbent to sub-erect, white  
487 to brown in color.

488 **Mandibles** Covered with white scales, with 3 longer setae, and 1 shorter seta between these.

489 **Rostrum** Length 0.50-0.59 mm, anterior portion ca. 1.5× broader than long, rostrum/pronotum length  
490 ratio 0.66-0.67, rostrum length/width ratio 1.43-1.48. Separation of rostrum from head generally obscure.  
491 Dorsal outline of rostrum nearly square, anterior half of dorsal surface mesally concave, posterior half  
492 coarsely but shallowly punctate to rugose. Rostrum in lateral view nearly square; apical margin bisinuate  
493 and emarginate, with 2 pairs of large vibrissae. Nasal plate defined by Y-shaped, impressed lines, convex,  
494 integument covered with white scales. Margins of mandibular incision directed ca. 15-20° outward  
495 dorsally in frontal view. Ventrolateral sulci strongly defined, beginning as a narrow sulcus posteriad of  
496 insertion point of mandibles, running parallel to scrobe, terminating in a ventral fovea.

497 **Antennae** Dorsal margin of scrobe overhanging broadly (not forming a minute tooth). Funicle slightly  
498 longer than scape. Scape extending *Brassieaceae* to posterior 1/4 of eye. Club nearly 3× as long as wide.

499 **Head** Eyes globular, anterodorsal margin of each eye impressed, posterior margin slightly elevated  
500 from lateral surface of head; eyes separated in dorsal view by 5× their anterior-posterior length, set off  
501 from anterior prothoracic margin by 1/4 of their anterior-posterior length. Head between eyes rugose and  
502 slightly bulging.

503 **Pronotum** Length/width ratio 0.85-0.87; widest near anterior 2/5. Anterior margin arcuate, subtly  
504 incurved mesally, and somewhat produced dorsally; anterior constriction broad, posterior margin slightly  
505 arcuate. Pronotum in lateral view with setae that reach beyond anterior margin; these setae becoming  
506 slightly longer and more erect laterally. Anterolateral margin with a reduced tuft of 3-6 post-ocular  
507 vibrissae present, emerging near ventral 1/2 of eye, and stopping just below ventral margin of eye;  
508 vibrissae varying in length from 1/2× anterior-posterior length of eye to a maximum length similar to  
509 anterior-posterior length of eye.

510 **Scutellum** Exposed, margins straight.

511 **Pleurites** Metepisternum nearly hidden by elytron except for triangular extension.

512 **Thoracic sterna** Mesocoxal cavities separated by 1/3× width of mesocoxal cavity. Metasternum with  
513 transverse sulcus not apparent; metacoxal cavities widely separated by ca. 2× their width.

514 **Legs** Profemur/pronotum length ratio 0.92-1.03; profemur with distal 1/6 produced ventrally as a  
515 slightly rounded, sub-rectangular projection covering tibial joint; condyle of tibial articulation occupying  
516 4/5 of distal surface and 1/6 length of femur. Protibia/profemur length ratio 0.87-0.93; protibial apex with  
517 ventral setal comb recessed in a subtly incurved groove; mucro not apparent. Protarsus with tarsomere III  
518 1.5× as long as II; wider than long. Metatibial apex with almond shaped convexity ringed by 10-12 short,  
519 spiniform setae.

520   **Elytra** Length/width ratio 3.12-3.16; widest at anterior 1/5; anterior margins jointly 1.5-2× wider  
521 than posterior margin of pronotum; lateral margins gently converging after anterior 1/5, more strongly  
522 converging in posterior 1/4. Posterior declivity angled at 65-70° to main body axis. Elytra with 10  
523 complete striae; striae broadly sculpted; punctures faint beneath appressed scales, separated by 5-7× their  
524 diameter; intervals elevated, with every second interval, beginning at elytral suture, more strongly raised  
525 than adjacent intervals.

526   **Abdominal sterna** Ventrite III anteromesally incurved around a fovea located mesally on anterior  
527 margin, posterior margin elevated and set off from IV along lateral 1/3s of its length. Sternum VII mesally  
528 2/3× as long as wide; anterior margin straight.

529   **Tergum** Pygidium sub-cylindrical; medial 1/2 of anterior 3/5 of pygidium less sclerotized.

530   **Sternum VIII** Anterior laminar edges of spiculum ventrale each incurved forming a 125° angle with  
531 lateral margin; lamina more sclerotized medially; posterior margin medially incurved.

532   **Ovipositor** Coxites as long as broad; styli as long as coxites, glabrous.

533   **Spermatheca** S-shaped; collum short, apically with a large, hood-shaped projection roughly aligned  
534 with central axis of corpus, nearly equal in length to bulb of ramus; collum sub-contiguous with, and  
535 angled at 30° to ramus; ramus elongate, sub-cylindrical to slightly bulbous, 3/4× thickness of corpus,  
536 with a short stalk oriented at ca. 45° to the corpus; corpus swollen, 1.3× thickness of ramus; cornu short,  
537 2.5-3× length of ramus, recurved and strongly arched in basal 1/2, forming an inner angle of ca. 80°,  
538 feebly sinuate thereafter, with apical 1/2 expanded, then abruptly constricted near apical 1/4 to a fine  
539 point.

540   **Description of male**

541 Similar to female, except where noted.

542   **Habitus** Length 3.10 mm, width 1.22 mm, length/width ratio 2.54. Rostrum length 0.53 mm, rostrum/pronotum length ratio 0.65, rostrum length/width ratio 1.66. Pronotum length/width ratio 0.99.  
543 Profemur/pronotum length ratio 1.01, protibia/profemur length ratio 0.82. Elytra length/width ratio 3.18.  
544

545   **Elytra** Elytral declivity slightly less angulate than female, forming a 60° angle to main body axis, but  
546 otherwise as in female.

547   **Abdominal sterna** Sternum VII 1/2× as long as wide, posterior margin feebly arcuate mesally.

548   **Tergum** Pygidium (tergum VIII) with mesal 1/3 of posterior margin subtly incurved; posterior 2/3  
549 punctate; anterior 1/3 rugose.

550   **Sternum VIII** Consisting of 2 sub-triangular sclerites; antero-laterally with a sharply-pointed projection  
551 as long as anterior-posterior length of triangular portion of sclerite.

552   **Aedeagus** Length/width ratio 7.00; lateral margins parallel, more strongly converging in region of  
553 ostium. In lateral view, width of pedon even throughout in anterior 2/3, ventral margins in posterior 1/3  
554 becoming straight towards apex, then curving to meet dorsal margins at a sharp apical point; apex acutely  
555 angulate. Flagellum without apparent sclerite.

556   **Comments**

557 Due to the limited number of specimens of this species, dissections of mouthparts could not be performed.

558   **Etymology**

559 Named in reference to the elevated elytral intervals, which give this species a sculpted appearance –  
560 *sculptilis* = “sculpted”; Latin adjective (Brown 1956).

561   **Material examined**

562   **Holotype** ♀ “Burley, Idaho; #7, 5-20-32; *A.[rtemisia] tridentata* [non-focal]; David E. Fox” (**USNM**).

563   **Paratypes** “Milner, Idaho; #5a, 7-9-31; *S.[alsola] pestifer*; David E. Fox” (**USNMCMNC**: 1 ♀); “Hazelton,  
564 Ida; #10 4/29/30; *N.[orta] altissima*” (**USNM**: 1 ♂)

565 **Distribution**

566 This species has been found in three localities along the Snake River in Idaho (USA), and is thought to be  
567 endemic to the Snake River Plain (Fig. 38).

568 **Natural history**

569 Associated with big sagebrush *Artemisia tridentata* Nutt. [non-focal] (Asteraceae [non-focal]), tumble-  
570 weed *Salsola tragus* L. [non-focal] (= *Salsola pestifer* A. Nelson [non-focal]) (Amaranthaceae [non-focal]),  
571 and tall tumblemustard *Sisymbrium altissimum* L. [non-focal] (= *Norta altissima* (L.) Britt. [non-focal])  
572 (Brassicaceae [non-focal]).

573 ***Minyomerus tylotos* Jansen & Franz sec. Jansen & Franz, 2018; sp. n.**

574 urn:lsid:zoobank.org:act:10CD3562-5969-4BCF-ACFE-BB0E5E2BF9A6

575 Figures 23-29

576 **Diagnosis**

577 *Minyomerus tylotos* [JF2018] is most readily distinguished from other congeners by a combination  
578 of characters, as follows. The nasal plate lacks distinct impressions, having instead a poorly defined  
579 anteromesal convexity completely and evenly covered with white scales. The frons is protuberant and  
580 moderately punctate. The entire body, including the legs, head, and venter, are clothed with brown,  
581 linear to minutely apically expanded setae, which are of similar length throughout and appear distinctly  
582 undifferentiated and uniform across body regions. The body is somewhat bulky, with the pronotum  
583 protuberant laterally and globular in dorsal view. The setae lining the anterodorsal margin of the pronotum  
584 uniquely apically explanate, with a longitudinal, medial, ridge-like portion that tapers to either side  
585 apicolaterally (visible at high magnification). The lateral margins of the elytra are protuberant anteriorly  
586 and sub-parallel along the between anterior 1/5 and posterior 1/3 of their length. The spermatheca has the  
587 corpus narrow throughout, equal in thickness to the collum. The ramus is basally stalked and apically  
588 bulbous. The collum exhibits a double-bend, and is recurved.

589 **Description of female**

590 **Habitus** Length 3.46-3.62 mm, width 1.42-1.54 mm, length/width ratio 2.35-2.44, widest at anterior  
591 1/6 of elytra. Integument orange-brown to black. Scales with variously interspersed colors ranging  
592 from slightly off-white or beige to manila/tan to dark coffee brown, in some specimens appearing  
593 semi-translucent (in others opaque). Setae linear to apically explanate, appearing minutely spatulate,  
594 sub-recumbent to sub-erect, tan to brown in color.

595 **Mandibles** Covered with white scales, with 2-3 longer setae, and 1-3 shorter setae between these.

596 **Maxillae** Cardo bifurcate at base with an inner angle of ca. 90°, arms roughly equal in length and  
597 width, arms of bifurcation equal in length to apically outcurved arm. Stipes sub-rectangular, 1.5× wider  
598 than long, roughly equal in width to inner arm of bifurcation of cardo, glabrous. Galeo-lacinial complex  
599 nearly extending to apex of maxillary palpomere I; complex mesally membranous, laterally sclerotized,  
600 with sharp demarcation of sclerotized region separating palpiger from galeo-lacinial complex; setose in  
601 membranous area just adjacent to sclerotized region, setae covering 1/2 of dorsal surface area; dorsally  
602 with 5 apicomosal lacinial teeth; ventrally with 3 reduced lacinial teeth. Palpiger with a single lateral seta,  
603 otherwise glabrous, anterior 1/2 membranous, posteriorly sclerotized.

604 **Maxillary palps** I apically oblique, apical end forming a 45° angle with base, with 2 apical setae; II  
605 sub-cylindrical, with 1 apical seta.

606 **Labium** Prementum roughly pentagonal; apical margins arcuate, medially angulate; lateral margins  
607 feebly incurved; basal margin arcuate. Labial palps 3-segmented, I with apical 1/2 projecting beyond  
608 margin of prementum, reaching apex of ligula; III slightly longer than II.

609 **Rostrum** Length 0.49-0.50 mm, anterior portion 2.25-2.5× broader than long, rostrum/pronotum length  
610 ratio 0.58-0.62, rostrum length/width ratio 1.26-1.32. Separation of rostrum from head generally obscure.  
611 Dorsal outline of rostrum nearly square, anterior half of dorsal surface feebly impressed, posterior half  
612 coarsely but shallowly punctate to rugose. Rostrum in lateral view nearly square; apical margin strongly  
613 bisinuate and emarginate, appearing medially notched, with 2 large vibrissae. Nasal plate lacking distinct  
614 impressions, having instead a poorly defined anteromesal convexity, integument completely and evenly

615 covered with white scales. Margins of mandibular incision directed ca. 25-30° outward dorsally in frontal  
616 view. Ventrolateral sulci weakly defined as a broad concavity dorsad of insertion point of mandibles,  
617 running parallel to scrobe, becoming flatter posteriorly and disappearing ventrally. Dorsal surface of  
618 rostrum with median fovea short and linear, or punctate. Rostrum ventrally with sub-parallel sulci  
619 beginning at corners of oral cavity and continuing halfway to back of head.

620 **Antennae** Minute tooth formed by overhanging dorsal margin of scrobe anterior to margin of eye by  
621 1/3 of length of eye. Scape extending to posterior margin of eye. Terminal funicular antennomere lacking  
622 appressed scales, having instead a covering of apically-directed pubescence with interspersed sub-erect  
623 setae. Club nearly 3× as long as wide.

624 **Head** Eyes globular and somewhat elongate, strongly impressed, slanted ca. 45° antero-ventrally; eyes  
625 separated in dorsal view by 4× their anterior-posterior length, set off from anterior prothoracic margin by  
626 1/4 of their anterior-posterior length. Head between eyes punctate and protuberant.

627 **Pronotum** Length/width ratio 0.88-0.89; widest near anterior 2/5; somewhat globular. Anterior margin  
628 arcuate, but feebly incurved mesally, lateral margins evenly curved and widening into a bulge just anteriad  
629 of midpoint of pronotum, posterior margin straight, with a slight mesal incurvature. Pronotum in lateral  
630 view with transverse ventrolateral sulci strongly excavated and distinctly sculptured; with short, recumbent  
631 to sub-erect setae that barely attain or reach just beyond anterior margin; these setae becoming shorter  
632 and more erect laterally, reaching a maximum length nearly equal to length of eye; dorsally, these setae  
633 become uniquely apically explanate, with a longitudinal, medial, ridge-like portion that tapers to either  
634 side apicolaterally. Anterolateral margin with a single ocular vibrissa present, emerging near ventral  
635 margin of eye; vibrissa achieving a maximum length of 2/5 of anterior-posterior length of eye.

636 **Scutellum** Not exposed.

637 **Pleurites** Metepisternum nearly hidden by elytron except for triangular extension.

638 **Thoracic sterna** Mesocoxal cavities separated by 1/3× width of mesocoxal cavity. Metasternum with  
639 transverse sulcus not apparent; metacoxal cavities widely separated by ca. 3× their width.

640 **Legs** Profemur/pronotum length ratio 0.90-0.96; profemur with distal 1/5 produced ventrally as a  
641 sub-rectangular projection covering tibial joint; condyle of tibial articulation occupying 4/5 of distal  
642 surface and 1/5 length of femur. Protibia/profemur length ratio 0.86-0.91; protibial apex with ventral setal  
643 comb recessed in a subtly incurved groove; mucro present as an acute, medially-projected tooth, which is  
644 approximately equal in length to surrounding setae. Protarsus with tarsomere III 2× as long as II; wider  
645 than long. Metatibial apex with weakly projecting, poorly defined, narrow convexity laterally flanged by  
646 5 short, spiniform setae.

647 **Elytra** Length/width ratio 3.03-3.21; widest at anterior 1/6; anterior margins jointly 1.5-2× wider  
648 than posterior margin of pronotum; lateral margins nearly straight and sub-parallel after anterior 1/5,  
649 converging in posterior 1/3. Posterior declivity angled at 70-75° to main body axis. Elytra with 10  
650 complete striae; striae broadly sculpted; punctures broad and faint beneath appressed scales, separated by  
651 4-5× their diameter; intervals elevated.

652 **Abdominal sterna** Ventricle III anteromesally incurved around a fovea located mesally on anterior  
653 margin, posterior margin elevated and set off from IV along lateral 3/8s of its length. Sternum VII mesally  
654 2/3× as long as wide; setae slightly lengthening, and becoming medially directed in posterior 1/3; anterior  
655 margin weakly curved; posterior margin distinctly incurved mesally, appearing broadly notched; surface  
656 of sternite concave, appearing broadly foveate, immediately anteriad of marginal incurvature.

657 **Tergum** Tergum VII mesally incurved. Pygidium sub-cylindrical; medial 1/3 of anterior 2/3 of pygidium  
658 less sclerotized, with a patch of very short, fine setae.

659 **Sternum VIII** Anterior laminar edges each incurved forming a 130° angle with lateral margin; slightly  
660 less sclerotized medially between arms; posterior margin medially incurved.

661 **Ovipositor** Coxites as long as broad; styli with 3 setae near the base.

662 **Spermatheca** ?-shaped; collum short, apically with a large, angulate, hood-shaped projection angled  
663 at 45° to corpus, sub-equal in length to ramus and contiously aligned with curvature of bulb of ramus;  
664 collum sub-contiguous with, and angled at ca. 60° to ramus; ramus basally elongate and constricted,  
665 forming a stalk, 1/3× length of collum, bulbous apically, 3× thicker than stalk; corpus not swollen, of  
666 equal thickness to collum and cornu; cornu elongate, apically, gradually narrowed, strongly recurved in  
667 basal 1/3, straight along mesal 1/3, and curved near apical 1/3 such that apex is parallel to collum and  
668 corpus.

669 **Description of male**

670 Not available or known.

671 **Etymology**

672 Named in reference to the short, apically explanate setae interspersed throughout the dorsum, which give  
673 this species a distinctly “knobbed” appearance; *tylotos* – knobby; Greek adjective (Brown 1956).

674 **Material examined**

675 **Holotype** ♀ “H. O. Canyon.; Davis Mts., Texas; Jeff Davis County; VII-20-1968, 6200’; J. E. Hafernink”  
676 (**TAMU**).

677 **Paratypes** “24 mi. wsw. Ft. Davis; Jeff Davis Co., Texas; August 17, 1969; Board & Hafernink” (**TAMU**:  
678 1 ♀); “USA Texas Jeff Davis Co.; 4.1 mi. S. Fort Davis; sweeping grasses-weeds; 4750’ . 19.VII.82; R.S.  
679 Anderson” (**CMNC**: 1 ♀)

680 **Distribution**

681 This species has been found in three localities near the Davis Mountains in Jeff Davis County and in nearby  
682 Presidio County, Texas (USA). Habitat models (Figs. 36) predict that this represents the northeastern  
683 extent of its range, indicating a strong likelihood that it is present in other parts of the northern Chihuahuan  
684 desert, especially in the state of Chihuahua (México).

685 **Natural history**

686 No host plant associations have been documented. It is unknown whether this species is parthenogenetic.

687 **CHECKLIST OF SPECIES**

688 RCC-5 articulations are provided in **bold font**. See Jansen & Franz (2015) for alignments of *Minyomerus*  
689 concepts published from 1831 to 2015.

*Minyomerus* Horn, 1876: 17 sec. Jansen & Franz (2018)

== (INT) AND > (**OST**) *Minyomerus* Horn, 1876 sec. Jansen & Franz (2015)

> AND = *Elissa* Casey, 1888: 271 sec. Casey (1888)

(synonymized by Kissinger, 1964: 30)

> AND = *Pseudelissa* Casey, 1888: 273 sec. Casey (1888)

(synonymized by Pierce, 1909: 359)

> AND = *Piscatopus* Sleeper, 1960: 84 sec. Sleeper (1960)

(synonymized by Jansen & Franz, 2015: 12)

*microps* (Say, 1831: 9) sec. Jansen & Franz (2015) [redescribed, p. 45]

== (INT) AND > (**OST**) AND = *Minyomerus innocuus* Horn, 1876: 18 sec. Horn (1876)

[former type of *Minyomerus*, designated by Pierce, 1913: 400]

(synonymized by Jansen & Franz, 2015: 45)

== (INT) AND > (**OST**) AND = *Thylacites microps* Say, 1831: 9 sec. Say (1831)

(transferred to *Minyomerus* on the authority of Buchanan *in litt.*

by Blackwelder and Blackwelder, 1948: 46)

== (INT) AND > (**OST**) AND = *Thylacites microsus* Boheman, 1833: 523 sec. Boheman (1833)

(synonymized by LeConte, 1859: 286)

*aeriballux* Jansen & Franz, 2015: 52 sec. Jansen & Franz (2015)

*ampullaceus* sp. nov. sec. Jansen & Franz (2018)

*bulbifrons* Jansen & Franz, 2015: 81 sec. Jansen & Franz (2015)

*caseyi* (Sharp, 1891: 151) sec. Jansen & Franz (2015) [redescribed, p. 66]

== AND = *Pseudelissa caseyi* Sharp, 1891: 151 sec. Sharp (1891)

(generic name synonymized by Pierce, 1909: 359)

*conicollis* Green, 1920: 194 sec. Jansen & Franz (2015) [redescribed, p. 33]

*constrictus* (Casey, 1888: 272) sec. Jansen & Franz (2015) [redescribed, p. 22]

== AND = *Elissa constricta* Casey, 1888: 272 sec. Casey (1888)

(generic name synonymized by Kissinger, 1964: 30)

*cracens* Jansen & Franz, 2015: 61 sec. Jansen & Franz (2015)

*franko* sp. nov. sec. Jansen & Franz (2018)

*gravivultus* Jansen & Franz, 2015: 92 sec. Jansen & Franz (2015)

*griseus* (Sleeper, 1960: 84) sec. Jansen & Franz (2015) [redescribed, p. 96]

== AND = *Piscatopus griseus* Sleeper, 1960: 84 sec. Sleeper (1960)

(generic name synonymized by Jansen & Franz, 2015: 96)

*imberbus* Jansen & Franz, 2015: 18 sec. Jansen & Franz (2015)

*languidus* Horn, 1876: 18 sec. Jansen & Franz (2015) [redescribed, p. 40]

== (INT) AND > (**OST**) *Minyomerus languidus* Horn, 1876: 18 sec. Horn (1876)

== AND = *Pseudelissa cinerea* Casey, 1888: 274 sec. Casey (1888)

(synonymized by Pierce, 1909: 359)

*laticeps* (Casey, 1888: 272) sec. Jansen & Franz (2015) [redescribed, p. 27]

== AND = *Elissa laticeps* Casey, 1888: 272 sec. Casey (1888)

(generic name synonymized by Kissinger, 1964: 30)

*politus* Jansen & Franz, 2015: 86 sec. Jansen & Franz (2015)

*puticulatus* Jansen & Franz, 2015: 75 sec. Jansen & Franz (2015)

*reburrus* Jansen & Franz, 2015: 57 sec. Jansen & Franz (2015)

*rutellirostris* Jansen & Franz, 2015: 103 sec. Jansen & Franz (2015)

*sculptilis* sp. nov. sec. Jansen & Franz (2018)

*trisetosus* Jansen & Franz, 2015: 71 sec. Jansen & Franz (2015)

*tylotos* sp. nov. sec. Jansen & Franz (2018)

690 **SPECIES IDENTIFICATION KEY**

- 1 Procoxae apparently separate, with intercoxal processes touching or very nearly so ..... 2
- Procoxae apparently contiguous, with intercoxal processes short and not touching ..... 3
- 2 (1) Rostrum approximately square and as wide as head in dorsal view; ramus of spermatheca basally narrow, forming a stalk that tapers into an apical bulb.....  
..... *Minyomerus rutellirostris* [JF2015]
- Rostrum approximately trapezoidal and narrower than the head in dorsal view; ramus of spermatheca cylindrical, somewhat bulbous, and basally constricted ..  
..... *Minyomerus griseus* [JF2015]
- 3 (1) Anterior margin of pronotum bearing a full, well-developed tuft of 10 or more ocular vibrissae; anterolateral margins of prementum explanate, angular, and posteriorly declivous, with a distinctly hexagonal appearance..... 4
- Ocular vibrissae reduced in number or length; anterior margins of prementum not explanate and declivous, typically with a pentagonal appearance ..... 5
- 4 (3) Head very wide and only somewhat swollen between eyes; rostrum ca. 4× wider than long in dorsal view; pronotum in dorsal view cylindrical; elytral setae short, brown, and sub-recumbent; ramus of spermatheca stalked and with apical bulb abruptly constricted, not tapering at point of connection to stalk ..... *Minyomerus laticeps* [JF2015]
- Head and rostrum typical (rostrum 2-3× wider than long in dorsal view); pronotum in dorsal view somewhat globular, with a strong anterior constriction; elytral setae short and setiform, especially near disk; spermatheca without basal stalk ..  
..... *Minyomerus constrictus* [JF2015]
- 5 (3) Metatibial apex strongly convex, with setae similar in length to those of remainder of leg, somewhat lighter in color and translucent, and slightly lamelliform; head somewhat conical in form, rounded between the eyes; elytral setae copious, not in uniform rows on intervals, instead appearing in offset rows, especially near elytral suture and declivity ..... 6
- Metatibial apex oblique or weakly convex, with setae short and conical in appearance; head roughly quadrate; elytral setae in relatively uniform rows on elytra, not strongly offset.... 7
- 6 (5) Elytral striae deeply and distinctly punctate, appearing pin-striped; elytra without obvious humeri, gradually widening posteriorly; ramus of spermatheca elongate, annulate, and sub-apically situated on corpus..... *Minyomerus aeriballux* [JF2015]
- Elytral striae punctate, with punctures somewhat obscured by appressed scales; elytra somewhat pyriform, with weak, but obviously present humeri; ramus of spermatheca elongate, somewhat swollen, and sub-apically situated on corpus ..  
..... *Minyomerus reburrus* [JF2015]
- 7 (5) Elytra very strongly convex in lateral view; anterior margin of pronotum wider than posterior margin; spermatheca comma-shaped, with ramus reduced, apically flattened and sub-contiguous with the collum; aedeagal pedon membranous ventrally, and not fully sclerotized ..  
..... *Minyomerus conicollis* [JF2015]
- Elytra only somewhat convex to nearly flat in lateral view; anterior margin of pronotum similar in length to posterior margin; spermatheca variable; aedeagal pedon fully sclerotized ..  
..... 8
- 8 (7) Body shape distinctly flask-like, with strongly constricted, sub-cylindrical pronotum and greatly protuberant elytra; in dorsal view, elytra nearly 2× width of pronotum at maximum width and nearly 3/4× as wide as long; in lateral view, anterior and posterior declivities of elytra abrupt and nearly vertical, with anterior elytral margin projecting strongly and characteristically dorsad of articulation with posterior pronotal margin; corpus of spermatheca with highly elongate projection aligned with midline of the ramus, which is basally tapered and angled at nearly 45° to corpus .. *Minyomerus ampullaceus* [JF2018], sp. n.

- Body shape usually narrow; elytra typically not more than  $1.5 \times$  width of pronotum and typically not more than  $2/3 \times$  as wide as long in dorsal view; elytral declivities in lateral view variable, but anterior margin never abruptly and strongly projected dorsad of posterior pronotal margin; spermatheca variable, but never with elongate projection aligned with midline of ramus ..... 9
- 9 (8) Setae of elytral disc a mix of shorter, brown setae and longer, more erect, white setae ..... 10
- Setae of elytral disc uniform ..... 12
- 10 (9) Anterior margin of pronotum bearing strikingly long setae, which project laterally up to  $80^\circ$  from longitudinal body axis and at least equal to diameter of eye; spermatheca with short, somewhat bulbous corpus, ramus sub-equal in size and perpendicular to corpus, and collum strongly recurved along basal  $1/3$  of its length; aedeagal pedon relatively short and wide, and abruptly constricted in apical  $1/5$ , thereafter tapered to rounded point ..... *Minyomerus franko* [JF2018], sp. n.
- Anterior margin of pronotum bearing setae more strongly directed anteriorly and never as long as diameter of eye; spermatheca variable; aedeagal pedon, where known, narrow and expanded laterally in region of ostium ..... 11
- 11 (10) Setae apically explanate, appearing somewhat spatulate; corpus of spermatheca uniquely elongate, ramus short and cylindrical ..... *Minyomerus caseyi* [JF2015]
- Setae linear; corpus of spermatheca typical, ramus bulbous and basally constricted ..... *Minyomerus trisetosus* [JF2015]
- 12 (9) Anterior margin of pronotum lined with linear setae that extend anteriorly beyond margin by half their length ..... 13
- 692 – Anterior margin of pronotum lacking setae, or with setae that do not extend far beyond margin ..... 14
- 13 (12) Lateral margins of gular cavity strongly rounded, never straight, and slightly longer than posterior margin; frons weakly projected between eyes; appressed scales on elytra without opalescent sheen; nasal plate with or without metallic reflections; lamina of spiculum ventrale sclerotized throughout ..... *Minyomerus languidus* [JF2015]
- Lateral margins of gular cavity nearly straight, and not longer than posterior margin; frons strongly projected between eyes; appressed scales with strong opalescent sheen; nasal plate with metallic reflections; lamina of spiculum ventrale with a membranous region present medially between laminar arm ..... *Minyomerus gravivultus* [JF2015]
- 14 (12) Elytra each  $4-5 \times$  as long as broad in dorsal view, strongly punctate; elytra constricted anteriad of humeri, narrower than the pronotum, widening thereafter near the humeri; spermatheca with the corpus somewhat bulbous, and the ramus either flattened somewhat or slightly elongate ..... *Minyomerus cracens* [JF2015]
- Elytra not so elongate, variably punctate; elytra lacking basal constriction; spermatheca variable ..... 15
- 15 (14) Elytral striae with large, obvious punctures ..... 16
- Elytral striae without evident punctures ..... 17
- 16 (15) Frons strongly protuberant; elytra in lateral view convex dorsally; spermatheca with corpus possessing an annulate, rectate projection nearly  $1/2 \times$  length of ramus; aedeagal pedon evenly curving towards apex; aedeagal flagellum with spiriform apical sclerite that spirals counterclockwise and of equal length to aedeagal pedon ..... *Minyomerus bulbifrons* [JF2015]

- Frons not so protuberant; elytra in lateral view nearly flat dorsally; spermatheca with corpus possessing an annulate, rectate projection nearly  $2/3 \times$  length of the ramus; aedeagal pedon narrow and elongate; aedeagal flagellum with very minute apical sclerite ..... *Minyomerus puticulatus* [JF2015]
- 17 (15) Frons strongly protruding in lateral view by ca.  $2 \times$  diameter of eye ..... 18
- Frons not or weakly protruding in lateral view by  $1.5 \times$  diameter of eye or less ..... 19
- 18 (17) Nasal plate defined by inversely V-shaped, impressed lines; spermatheca with the ramus elongate and apically swollen, corpus possessing an annulate, rectate projection nearly  $1/2 \times$  length of the ramus, and cornu evenly recurved throughout its length; aedeagal flagellum with a spiriform apical sclerite that spirals clockwise and of equal length to pedon ..... *Minyomerus politus* [JF2015]
- Nasal plate lacking distinct impressions; spermatheca with ramus basally tapered with a short stalk, corpus narrow and lacking an annulate rectate bulb, and cornu with an abrupt apical curve; males not known ..... *Minyomerus tylotos* [JF2018], sp. n.
- 19 (17) Ventrolateral sulci weakly defined as a notch ventrad of antennal insertion, or absent entirely; intervals broadly sculpted and raised, and striae not punctate; body generally robust in overall quality; appressed scales uniformly beige and gray, with a distinctly ‘crusty’ appearance; spermatheca with ramus and collum appearing as two subcontiguous, apically invaginated bulbs ..... *Minyomerus microps* [JF2015]
- Ventrolateral sulci deeply and distinctly defined along their entire length; intervals, if raised, only sculpted along lateral faces of elytra, not on disk; body usually not markedly robust; appressed scales either translucent or otherwise typical of genus, not beige and crusted; spermatheca distinctly sinuate, with well defined, protruding ramus ..... 20
- 20 (19) Elytra with very minute setae, only perceptible at high magnification; lateral faces of elytra with intervals not noticeably raised; ramus of spermatheca elongate, cylindrical, and slightly thinner than corpus, cornu strongly recurved in basal half with uniquely sinuate appearance, both corpus and cornu with hood-like projections shorter than ramus; males not known ..... *Minyomerus imberbus* [JF2015]
- Elytra with easily visible, linear setae; lateral faces of elytra with intervals raised; ramus of spermatheca bulbous, basally tapered, and similar in width to corpus, cornu strongly recurved, but short in basal half with uniquely sinuate appearance, both corpus and cornu with hood-like projections longer than ramus; aedeagal pedon narrow and cylindrical, apically tapered ..... *Minyomerus sculptilis* [JF2018], sp. n.

## 694 PHYLOGENETIC RESULTS

695 A matrix of 52 characters was assembled for the 26 terminal taxa (Tab. 1). These characters are comprised  
 696 of all 46 characters included in the revision of *Minyomerus* [JF2015], plus an additional 6 characters  
 697 intended to identify putative sister taxa to the newly described species. Parsimony analysis returned a  
 698 single, most-parsimonious cladogram (henceforth MPT) with a length (L) of 99 steps, a consistency index  
 699 (CI) of 60 and a retention index (RI) of 80 (Farris 1989); see Figs. 30-31. TNT (Tree Analysis Using  
 700 New Technology) was used to confirm that the shortest tree had been found (Goloboff et al. 2008). The  
 701 most-parsimonious cladogram is shown in Fig. 30, with relative and absolute Bremer support values  
 702 (see also **Materials and Methods: Phylogenetic analysis**) mapped along the left side of each branch;  
 703 nodes with bootstrap support above 0.95 are marked with a “\*” symbol to the right of each node. In a  
 704 complementary graph, we show the herein used clade concept labels (Fig. 31).

705 The characters, states, and preferred optimizations are described in this section. Characters relating  
 706 to placement of the herein described taxa are discussed in detail in the **Discussion** section, along with  
 707 changes in species group composition and tree topology from Jansen & Franz (2015). For all characters  
 708 not resolved as unreversed synapomorphies, both the individual consistency (ci) and retention (ri) indices  
 709 are provided. ~~Characters are numbered in accordance with descriptive sequence used in the species~~  
 710 ~~accounts. A “—” symbol indicates inapplicable (character, state), whereas a “?” symbol indicates missing~~  
 711 ~~information, e.g., due to the unavailability of male specimens or insufficient specimens on hand to permit~~  
 712 ~~full dissections. Characters 9, 27, 39, 45–47, 49, and 51 were mapped onto the preferred phylogeny~~  
 713 ~~using ACCTRAN optimization (see Agnarsson & Miller 2008), and the remaining characters had an~~  
 714 ~~unambiguous optimization.~~

**Table 1. Taxon/character matrix used for for cladistic analysis.** Includes all species of *Minyomerus* [JF2015], newly designated species, and select outgroup taxa. All multi-state characters coded as additive, except for character 33. The symbol “—” denotes inapplicable character states, whereas “?” denotes missing information (see also text).

TAXON \ CHARACTER	0 5	1 0	1 5	2 0	2 5	3 0	3 5	4 0	4 5	5 0
<i>Sitona californicus</i> [non-focal]	00-00	?????	00000	00000	00000	00000	00---	-0---	--???	?????
<i>Pandeleteius cinereus</i> [non-focal]	11000	?????	01000	00001	01000	00100	00000	000-0	00???	?????
<i>Pandeleteius subcancer</i> [non-focal]	11000	?????	01000	00001	01010	00100	00000	000-0	00???	?????
<i>Isodrusus debilis</i> [non-focal]	11000	?????	01000	00001	01011	00100	00000	000-0	00???	?????
<i>Isodacrys buchanani</i> [non-focal]	11000	?????	01000	00001	01011	00101	00000	000-0	00???	?????
<i>Minyomerus constrictus</i> [JF2015]	21100	00010	02110	01002	00011	11211	00000	00000	00000	01010 00
<i>Minyomerus laticeps</i> [JF2015]	21100	00010	02110	01002	00011	11211	00000	00000	00000	01010 00
<i>Minyomerus imberbus</i> [JF2015]	21100	?????	02010	11002	10011	11211	01001	00000	00???	?????
<i>Minyomerus sculptilis</i> [JF2018]	21100	?????	02010	11002	10011	11211	01001	00000	00001	00000 10
<i>Minyomerus conicollis</i> [JF2015]	21100	00000	02010	11002	10011	10211	00001	10000	01000	00000 00
<i>Minyomerus languidus</i> [JF2015]	21000	11100	02010	11002	10011	10211	00001	10000	?????	????? ??
<i>Minyomerus microps</i> [JF2015]	21001	11101	02110	11002	10011	10211	00001	10000	10???	????? ??
<i>Minyomerus tylopus</i> [JF2018]	21001	11101	02110	11002	10011	10211	00001	10000	00???	????? ??
<i>Minyomerus cracens</i> [JF2015]	21000	11101	02020	11112	10011	11211	00001	10001	00000	10010 10
<i>Minyomerus ampullaceus</i> [JF2018]	21000	?????	02020	111?2	10011	11211	00001	11001	00???	????? ??
<i>Minyomerus aeriballus</i> [JF2015]	22000	11101	12020	11012	10011	20211	00001	11001	10000	00000 01
<i>Minyomerus reburrus</i> [JF2015]	22000	11101	12020	11112	10011	20211	00001	11021	00???	????? ??
<i>Minyomerus franko</i> [JF2018]	21110	10100	02020	11002	10011	11211	00001	10011	10010	00000 01
<i>Minyomerus caseyi</i> [JF2015]	21110	00101	02020	11112	10011	11211	00001	10101	10010	10010 01
<i>Minyomerus trisetosus</i> [JF2015]	21110	00101	02020	11012	10011	10211	00001	10101	10???	????? ??
<i>Minyomerus gravivulvus</i> [JF2015]	21100	11101	02120	11002	10011	10211	00111	10000	?010	00000 11
<i>Minyomerus griseus</i> [JF2015]	21100	10101	02120	01002	10111	11211	00111	10000	00010	01100 10
<i>Minyomerus rutellirostris</i> [JF2015]	21100	10101	02120	11002	10111	11211	00111	10000	00010	01100 10
<i>Minyomerus puticalatus</i> [JF2015]	21000	11101	02020	11012	10011	11211	10101	10010	01011	01000 11
<i>Minyomerus bulbifrons</i> [JF2015]	21000	11101	02021	11112	10011	10211	10101	10000	01110	01001 01
<i>Minyomerus politus</i> [JF2015]	21000	?????	02021	11112	10011	10211	10101	10010	01111	01001 11

- 715 1. Habitus, form of appressed scales: (0) elongate pyriform, not overlapping; (1) sub-circular to  
 716 polygonal, variously overlapping non-linearly; (2) sub-circular and only overlapping posteriorly.  
 717 Coded as additive due to alignment of character states with the preferred phylogeny. Coding as  
 718 non-additive in isolation or in unison with other additive multi-state characters does not affect  
 719 polarization of the character/states or alter the phylogeny. State 1 is a synapomorphy for the  
 720 tanymeyeine clade [non-focal], whereas state 2 is a synapomorphy for *Minyomerus* [JF2018].

- 721        2. Habitus, arrangement of elytral setae: (0) variously interspersed; (1) arranged in single-file rows  
 722        on elytral intervals; (2) arranged non-uniformly on elytral intervals. Coded as additive due to  
 723        alignment of character states with the preferred phylogeny. Coding as non-additive in isolation or in  
 724        unison with other additive multi-state characters does not affect polarization of the character/states  
 725        or alter the phylogeny. State 1 is a synapomorphy for the tanytomecine clade [non-focal], whereas  
 726        state 2 is a synapomorphy for the *M. aeriballus*–*M. reburrus* clade [JF2015].
- 727        3. Habitus, lateral elytral setae and ventral setae differentiated from setae of elytral disc: (0) absent;  
 728        (1) present. Homoplasy for *Minyomerus* [JF2018], with a reversal (state 0) in the *M. aeriballus*–*M.*  
 729        *languidus* clade [JF2015], subsequent convergent gain (state 1) in the *M. bulbifrons*–*M. caseyi* clade  
 730        [JF2018], and convergent reversal (state 0) in the *M. bulbifrons*–*M. puticalutus* clade [JF2015] (ci =  
 731        25; ri = 70).
- 732        4. Habitus, rows of elytral setae with larger white setae randomly interspersed among smaller brown  
 733        setae: (0) absent; (1) present. Synapomorphy for the *M. caseyi*–*M. franko* clade [JF2018]. Changed  
 734        from Jansen & Franz (2015), where *M. rutellirostris* [JF2015] was previously coded as having this  
 735        character; however, the white elytral setae of this species are not randomly interspersed, but follow  
 736        a distinct, and uniquely derived, pattern where every other interval contains a row of such setae.
- 737        5. Habitus, elytra and pronotum generally large, protuberant, and sculpted in appearance along dorsal  
 738        and lateral faces: (0) absent; (1) present. Synapomorphy for the *M. microps*–*M. tylotos* clade  
 739        [JF2018].
- 740        6. Prementum, anterior margin ~~forming a distinct face medially with a distinct facet, rather than a~~  
 741        ~~single edge~~, that continues to lateral margins: (0) absent; (1) present. Synapomorphy for the  
 742        *M. aeriballus*–*M. languidus* clade [JF2015], with a single reversal in the *M. caseyi*–*M. trisetosus*  
 743        clade [JF2015] (ci = 50; ri = 75).
- 744        7. Prementum, strongly ligulate and with margins nearly straight, appearing pentagonal: (0) absent;  
 745        (1) present. Synapomorphy for the *M. aeriballus*–*M. languidus* clade [JF2015], with independent  
 746        reversals in the *M. caseyi*–*M. franko* clade [JF2018] and *M. griseus*–*M. rutellirostris* clade [JF2015],  
 747        respectively (ci = 33; ri = 71).
- 748        8. Prementum, anterolateral margins simple, unexpanded: (0) absent; (1) present. Synapomorphy for  
 749        the *M. aeriballus*–*M. languidus* clade [JF2015].
- 750        9. Prementum, anterolateral margins explanate, angular, and posteriorly declivous, with a distinctly  
 751        hexagonal appearance: (0) absent; (1) present. ACCTRAN optimization preferred (see Agnarsson  
 752        & Miller 2008), therefore inferred as a synapomorphy for the *M. constrictus*–*M. laticeps* clade  
 753        [JF2015].
- 754        10. Prementum, exposure of palpomere I: (0) exposed, visible beyond ligula and anterior margin of  
 755        prementum in ventral view; (1) hidden, fully covered or only minutely exposed beyond ligula and  
 756        anterior margin of prementum in ventral view. Synapomorphy for the *M. aeriballus*–*M. microps*  
 757        clade [JF2015], with a single reversal in *M. franko* [JF2018] (ci = 50; ri = 75).
- 758        11. Rostrum, form in dorsal view: (0) approximately quadrate; (1) somewhat conical, medially convex.  
 759        Synapomorphy for the *M. aeriballus*–*M. reburrus* clade [JF2015].
- 760        12. Rostrum, form of nasal plate and demarcation of epistoma: (0) with three parallel, longitudinal cari-  
 761        nae, and surface planar between these; (1) with a sharp, narrow, chevron-shaped carina demarcating  
 762        epistoma; (2) with a broad, scale-covered, chevron-shaped carina demarcating epistoma. Coded  
 763        as additive due to alignment of character states with preferred phylogeny. Coding as non-additive  
 764        in isolation or in unison with other additive multi-state characters does not affect polarization of  
 765        the character/states or alter the phylogeny. State 1 is a synapomorphy for the tanytomecine clade  
 766        [non-focal], whereas state 2 is a synapomorphy for *Minyomerus* [JF2018].
- 767        13. Rostrum, sulcus posteriad of nasal plate weakly impressed: (0) absent; (1) present. Convergently  
 768        present in the *M. constrictus*–*M. laticeps* clade [JF2015], the *M. microps*–*M. tylotos* clade [JF2018],  
 769        and the *M. gravivultus*–*M. griseus* clade [JF2015] (ci = 33; ri = 60).

- 770 14. Rostrum, form of sulcus posteriad of nasal plate: (0) absent; (1) sulcus present, broad, and weakly  
771 punctate; (2) sulcus present, more strongly punctate. Coded as additive due to alignment of character  
772 states with preferred phylogeny. Coding as non-additive in isolation or in unison with other additive  
773 multi-state characters does not affect polarization of the character/states or alter the phylogeny.  
774 Synapomorphy for *Minyomerus* [JF2018] (state 1) and the *M. aeriballux*–*M. cracens* clade [JF2015]  
775 (state 2), respectively.
- 776 15. Head, frons very strongly projected beyond anterior margin of eye, by 2× anterior-posterior length  
777 of eye: (0) absent; (1) present. Synapomorphy for the *M. bulbifrons*–*M. politus* clade [JF2015].
- 778 16. Head, frons with posterior transverse constriction: (0) absent; (1) present. Synapomorphy for the *M.*  
779 *aeriballux*–*M. languidus* clade [JF2015], with a single reversal in *M. griseus* [JF2015] (ci = 50, ri =  
780 85).
- 781 17. Antenna, length of scrobe relative to funicle and club: (0) scrobe shorter than funicle and club com-  
782 bined; (1) scrobe subequal in length to funicle and club combined. Synapomorphy for *Minyomerus*  
783 [JF2018].
- 784 18. Antenna, terminal funicular segment entirely without thin, nearly setiform scales: (0) absent; (1)  
785 present. Convergently present in *M. cracens* [JF2015], *M. reburrus* [JF2015], *M. caseyi* [JF2015],  
786 and the *M. bulbifrons*–*M. politus* clade [JF2015] (ci = 25; ri = 25).
- 787 19. Antenna, terminal funicular segment at least partially clothed with broad scales: (0) absent; (1)  
788 present. Synapomorphy for the *M. aeriballux*–*M. cracens* clade [JF2018] with independent reversals  
789 in *M. franko* [JF2018] and the *M. gravivultus*–*M. griseus* clade [JF2015] (ci = 33; ri = 71).
- 790 20. Head, angle of base in relation to prothorax: (0) directed anteriorly, in line with main body axis; (1)  
791 directed strongly ventrally; (2) directed slightly ventrally. Coded as additive due to alignment of  
792 character states with preferred phylogeny. Coding as non-additive in isolation or in unison with  
793 other additive multi-state characters does not affect polarization of the character/states or alter the  
794 phylogeny. State 1 is a synapomorphy for the tanymecine clade [non-focal], whereas state 2 is a  
795 synapomorphy for *Minyomerus* [JF2018].
- 796 21. Pronotum, condition of post-ocular vibrissae: (0) present in a well-developed tuft of 10 or more  
797 setae; (1) present in a reduced tuft of 3–7 setae. Synapomorphy for the *M. aeriballux*–*M. imberbus*  
798 clade [JF2018].
- 799 22. Prosternum, intercoxal process complete, undivided: (0) absent; (1) present. Synapomorphy for the  
800 tanymecine clade [non-focal], with a single reversal for *Minyomerus* [JF2018] (ci = 50; ri = 66).
- 801 23. Prosternum, intercoxal process divided at midpoint between coxae, but both anterior and posterior  
802 processes extending completely between procoxae and contiguous with each other: (0) absent; (1)  
803 present. Synapomorphy for the *M. griseus*–*M. rutellirostis* clade [JF2015].
- 804 24. Legs, fore femora not swollen in comparison to other legs: (0) absent; (1) present. Synapomorphy  
805 for the *M. aeriballux*–*P. subcancer* clade [non-focal].
- 806 25. Legs, sculpture of ventral surface of protibiae: (0) evenly convex throughout; (1) with a longitudinal  
807 groove or concavity. Synapomorphy for the *M. aeriballux*–*I. debilis* clade [non-focal].
- 808 26. Legs, setation of metatibial apex: (0) bristles at least as long as surrounding setae and setiform; (1)  
809 bristles shorter than surrounding setae and conical; (2) bristles sub-equal in length to surrounding  
810 setae and somewhat lamelliform. Coded as additive due to alignment of character states with  
811 preferred phylogeny, and the appearance of being a transformation series. Coding as non-additive  
812 in isolation or in unison with other additive multi-state characters does not affect polarization of the  
813 character/states or alter the phylogeny. Synapomorphy for *Minyomerus* [JF2018] (state 1) and the  
814 *M. aeriballux*–*M. reburrus* clade [JF2015] (state 2), respectively.

- 815 27. Legs, curvature of metatibial apex: (0) convex ; (1) oblique. ACCTRAN optimization preferred  
 816 (see Agnarsson & Miller 2008), therefore inferred as a synapomorphy for *Minyomerus* [JF2018]  
 817 with a reversal (state 0) in the *M. aeriballux*–*M. conicollis* clade [JF2015], then a convergent gain  
 818 (state 1) in the *M. aeriballux*–*M. bulbifrons* clade [JF2018], with independent reversals (state 0) in  
 819 the *M. aeriballux*–*M. reburrus* clade [JF2015], *M. gravivultus* [JF2015], *M. trisetosus* [JF2015],  
 820 and the *M. bulbifrons*–*M. politus* clade [JF2015] (ci = 14; ri = 40).
- 821 28. Legs, relative length of mesotarsi to mesotibiae: (0) tarsi ~~much shorter than~~less than  $\frac{3}{4} \times$  length  
 822 of tibiae; (1) tarsi at least equal in length to tibiae; (2) tarsi ~~slightly~~ shorter than tibiae, but longer  
 823 than  $\frac{3}{4} \times$  length of tibiae. Coded as additive due to alignment of character states with preferred  
 824 phylogeny. Coding as non-additive in isolation or in unison with other additive multi-state characters  
 825 does not affect polarization of the character/states or alter the phylogeny. State 1 is a synapomorphy  
 826 for the tanymeyeine clade [non-focal], whereas state 2 is a synapomorphy for *Minyomerus* [JF2018].
- 827 29. Legs, tarsi ventrally spinose: (0) absent; (1) present. Synapomorphy for *Minyomerus* [JF2018].
- 828 30. Elytra, humeral angle rounded, not projected: (0) absent; (1) present. Synapomorphy for the *M.*  
 829 *aeriballux*–*I. buchanani* clade [non-focal].
- 830 31. Female terminalia, spermatheca with apical cylindrical bulb on corpus: (0) absent; (1) present.  
 831 Synapomorphy for the *M. bulbifrons*–*M. puticulatus* clade [JF2015].
- 832 32. Female terminalia, corpus of spermatheca sinuate: (0) absent; (1) present. Synapomorphy for the  
 833 *M. imberbus*–*M. sculptilis* clade [JF2018].
- 834 33. Female terminalia, lamina of spiculum ventrale less sclerotized between laminar arms: (0) absent;  
 835 (1) present. Coded as inapplicable for *S. californicus* [non-focal], as laminar arms are not apparent.  
 836 Synapomorphy for the *M. gravivultus*–*M. griseus* clade [JF2015].
- 837 34. Female terminalia, lamina of spiculum ventrale with laminar arms bifurcating around a membranous  
 838 region: (0) absent; (1) present. Coded as inapplicable for *S. californicus* [non-focal], as laminar  
 839 arms are not apparent. Synapomorphy for the *M. gravivultus*–*M. griseus* clade [JF2015].
- 840 35. Female terminalia, lamina of spiculum ventrale with style basally divided or obscured, not mesally  
 841 intact: (0) absent; (1) present. Coded as inapplicable for *S. californicus* [non-focal], as laminar  
 842 arms are not apparent. Synapomorphy for the *M. aeriballux*–*M. imberbus* clade [JF2015].
- 843 36. Female terminalia, lamina of spiculum ventrale with laminar arms clearly bifurcating. (0) absent;  
 844 (1) present. Coded as inapplicable for *S. californicus* [non-focal], as laminar arms are not apparent.  
 845 Synapomorphy for the *M. aeriballux*–*M. conicollis* clade [JF2015].
- 846 37. Female terminalia, laminar arms narrowly bifurcating basally, thereafter sub-parallel mesally: (0)  
 847 absent; (1) present. Synapomorphy for the *M. aeriballux*–*M. ampullaceus* clade [JF2018].
- 848 38. Female terminalia, coxites of ovipositor with a lateral, anteriorly-directed, recurved, alate process:  
 849 (0) absent; (1) present. Coded as inapplicable for *S. californicus* [non-focal], as coxites of ovipositor  
 850 are not apparent. Synapomorphy for the *M. caseyi*–*M. trisetosus* clade [JF2015].
- 851 39. Female terminalia, relative length of styli to coxites of ovipositor: (0) Similar in size; (1) distinctly  
 852 shortened; (2) highly reduced, appearing minute. Coded as non-additive, due to strong differences  
 853 in structure of coxites and styli in state 2; inapplicable for outgroup taxa, as styli of ovipositor are  
 854 not apparent. ACCTRAN optimization preferred (see Agnarsson & Miller 2008), therefore inferred  
 855 as convergent gains in *M. franko* [JF2018] and the *M. bulbifrons*–*M. puticulatus* clade [JF2015]  
 856 (state 1), with a single reversal in *M. bulbifrons* [JF2015] (state 0). Autapomorphy for *M. reburrus*  
 857 [JF2015] (state 2) (ci = 50, ri = 0).
- 858 40. Female terminalia, condition of medial, anteriorly-directed, sclerotized process of coxites of  
 859 ovipositor: (0) fully developed; (1) reduced and inapparent. Coded as inapplicable for *S. californicus*  
 860 [non-focal], as coxites of ovipositor are not apparent. Synapomorphy for the *M. aeriballux*–*M.*  
 861 *cracens* clade [JF2015], with a single reversal in the *M. gravivultus*–*M. griseus* clade [JF2015] (ci  
 862 = 50, ri = 83).

- 863 41. Female terminalia, anterior margin of tergum VII entirely free of sclerotized band: (0) absent;  
864 (1) present. Coded as inapplicable for *S. californicus* [non-focal], as the tergum VII is evenly  
865 sclerotized throughout. Convergently present in *M. aeriballux* [JF2015], *M. microps* [JF2015], and  
866 the *M. caseyi*–*M. trisetosus* clade [JF2018] (ci = 33; ri = 50).

867 42. Female terminalia, anterior margin of tergum VII sclerotized fully, appearing as an obviously  
868 complete band: (0) absent; (1) present. Coded as inapplicable for *S. californicus* [non-focal], as the  
869 tergum VII is evenly sclerotized throughout. Convergently present in *M. conicollis* [JF2015] and  
870 the *M. bulbifrons*–*M. puticulatus* clade [JF2015] (ci = 50; ri = 66).

871 43. Male terminalia, apical sclerite of aedeagal flagellum elongate-spiriform: (0) absent; (1) present.  
872 Synapomorphy for the *M. bulbifrons*–*M. politus* clade [JF2015].

873 44. Male terminalia, style of spiculum gastrale with an anterior ventral flange: (0) absent; (1) present.  
874 Synapomorphy for the *M. bulbifrons*–*M. caseyi* clade [JF2018].

875 45. Male terminalia, lamina of spiculum gastrale longer than broad and anteriorly extended along  
876 style: (0) absent; (1) present. ACCTRAN optimization preferred (see Agnarsson & Miller 2008),  
877 therefore inferred as convergent gains in the *M. imberbus*–*M. sculptilis* clade [JF2018] and the *M.*  
878 *bulbifrons*–*M. puticulatus* clade [JF2015], with a reversal in *M. bulbifrons* [JF2015] (ci = 33; ri =  
879 0).

880 46. Male terminalia, sub-triangular sclerites of sternum VIII with a medial process: (0) absent; (1)  
881 present. ACCTRAN optimization preferred (see Agnarsson & Miller 2008), therefore inferred as  
882 convergent gains in *M. cracens* [JF2015] and the *M. caseyi*–*M. trisetosus* clade [JF2015] (ci =  
883 50, ri = 0).

884 47. Male terminalia, curvature of posterior margin of tergum VII: (0) evenly arcuate; (1) medially  
885 incurved. ACCTRAN optimization preferred (see Agnarsson & Miller 2008), therefore convergently  
886 present in the *M. constrictus*–*M. laticeps* clade [JF2015] and the *M. bulbifrons*–*M. gravivultus* clade  
887 [JF2015] with a reversal in *M. gravivultus* [JF2015] (ci = 33; ri = 66).

888 48. Male terminalia, tergum VII approximately 4× as long as broad: (0) absent; (1) present. Synapo-  
889 mophy for the *M. griseus*–*M. rutellirostris* clade [JF2015].

890 49. Male terminalia, aedeagal pedon expanded laterally around ostium: (0) absent; (1) present. ACC-  
891 TRAN optimization preferred (see Agnarsson & Miller 2008), therefore convergently present in the  
892 *M. constrictus*–*M. laticeps* clade [JF2015], *M. cracens* [JF2015], and the *M. caseyi*–*M. trisetosus*  
893 clade [JF2015] (ci = 33; ri = 33).

894 50. Male terminalia, aedeagal pedon broad basally, evenly tapering toward apex: (0) absent; (1) present.  
895 Synapomorphy for the *M. bulbifrons*–*M. politus* clade [JF2015].

896 51. Male terminalia, aedeagal pedon medially sclerotized along dorsum: (0) absent; (1) present.  
897 ACCTRAN optimization preferred (see Agnarsson & Miller 2008), therefore convergently present  
898 in the *M. imberbus*–*M. sculptilis* clade [JF2015], *M. cracens* [JF2015], and the *M. bulbifrons*–*M.*  
899 *gravivultus* clade [JF2015], with a reversal in *M. bulbifrons* [JF2015] (ci = 25; ri = 50).

900 52. Male terminalia, width of connection between apodemes of aedeagal tegmen: (0) wider than base of  
901 apodeme; (1) narrower than base of apodeme. Synapomorphy for the *M. aeriballux*–*M. bulbifrons*  
902 clade [JF2018], with a single reversal in the *M. griseus*–*M. rutellirostris* clade [JF201] (ci = 50; ri  
903 = 83).

## RCC-5 ALIGNMENTS

Details of our RCC-5 alignment approach are given in free text form in the **Supplemental Information SI1**, which also describes the content of the data input and output files. The latter, in turn, are appended in .txt, .csv, and .pdf format in the **Supplemental Information SI2 to S4**. All shown alignments are *intensional* in the sense of Franz & Peet (2009), and thus maximize high-level concept congruence where indicated, and in spite of non-congruent lower-level concept sampling.

910 The first, classification-based alignment (Fig. 32) is simple and straightforward to interpret (see also  
911 **Supplemental Information SI2**). We obtain high-level congruence among the concepts *Minyomerus*  
912 [JF2018] and *Minyomerus* [JF2015], where 17 species-level concepts are retained from Jansen & Franz  
913 (2015) and four species-level concepts are added in the current ~~revision~~review. The coverage constraint  
914 is relaxed for *Minyomerus* [JF2015], thus allowing the four new species-level concepts to be subsumed  
915 under this parent. This is based on our assertion that they fall under the generic character circumscription  
916 of Jansen & Franz (2015).

917 The following two Figs. 33-34 show fully bifurcated, multi-phylogeny alignments of the same reasoner  
918 toolkit input, but resolved as whole concepts versus split concepts, respectively. In Fig. 33 (**Supplemental**  
919 **Information SI3**), we observe that the phylogenetic placements of *two* of the four new species-level  
920 concepts cause significant non-congruence in the alignment, resulting in seven overlapping RCC-5  
921 articulations. *Minyomerus franko* [JF2018] is subsumed under the *M. caseyi*-*M. franko* clade [JF2018],  
922 which is intensionally congruent with the *M. caseyi*-*M. trisetosus* clade [JF2015]. In other words, this  
923 placement is not the source of non-congruence in the alignment. Similarly, the placement of *M. tylotos*  
924 [JF2018] into the new *M. microps*-*M. tylotos* clade [JF2018] is not conflicting in an intensional sense. At  
925 the next, more inclusive level, this addition "resolves" into the congruent *M. aeriballux*-*M. microps* clade  
926 [JF2018]/[JF2015].

927 In contrast, the placement of *M. ampullaceus* [JF2018] "inside" of *M. cracens* [JF2015] in the current  
928 phylogeny, generates five overlapping articulations among as many (five) non-congruent concept regions  
929 positioned 1-2 levels above these species-level concepts. The conflict is resolved in the next, more  
930 inclusive and congruent region of the *M. aeriballux*-*M. cracens* clade [JF2018] == *M. aeriballux*-*M.*  
931 *bulbifrons* clade [JF2015]

932 The placements of the previously circumscribed *M. imberbus* [JF2015] and the new species-level con-  
933 cept *M. sculptilis* [JF2018] - in relation to the congruent clade *M. constrictus*-*M. laticeps* [JF2018]/[JF2015]  
934 - cause two additional instances of overlap (Fig. 33). In the current phylogeny, *M. imberbus* [JF2015] is sis-  
935 ter to *M. sculptilis* [JF2018], and placed "inside" of the *M. constrictus*-*M. laticeps* clade [JF2018]/[JF2015].  
936 However, in the preceding phylogeny sec. Jansen & Franz (2015), *M. imberbus* [JF2015] is non-  
937 congruently included in the *M. constrictus*-*M. imberbus* clade [JF2015]. This conflict is only resolved at  
938 the level of *Minyomerus* [JF2018]/[JF2015].

939 Figure 34 (**Supplemental Information SI4**) shows that the inclusion of the four new species-level  
940 concepts in the *Minyomerus* [JF2018] phylogeny generates five split-concept regions for which there are  
941 no adequate labels in either input phylogeny. These labels correspond to the overlapping articulations  
942 mentioned above; in particular the non-congruent assignments of *M. ampullaceus* [JF2018], *M. cracens*  
943 [JF2018], and *M. sculptilis* [JF2018]. The phylogenetic character evidence for these placements and  
944 relationships are discussed in the following sections.

## 945 DISCUSSION

### 946 Relationships to the previous revision

947 The differences of the current phylogeny (Figs. 30-31) in relation to that of Jansen & Franz (2015) are in  
948 large part due to the unique character combinations present in the newly added species (Rieppel 2007,  
949 Franz 2014). Nonetheless, three main clades are resolved with strong support, and further corroborate the  
950 topology of Jansen & Franz (2015), as follows:

- 951 1. *Minyomerus* [JF2018] is strongly supported by the same eight synapomorphies identified in Jansen  
952 & Franz (2015). These are reiterated in the Introduction (Bremer support value [henceforth: bsv] =  
953 10, relative fit difference [henceforth: rfd] = 95; Bootstrap [henceforth: boot] = 100).
- 954 2. *Minyomerus griseus* [JF2015] forms a well-supported clade with *M. rutellirostris* [JF2015] (bsv =  
955 4, rfd = 77, boot = 96). These taxa jointly share the same two synapomorphies (chars. 23:1 and  
956 48:1) provided in Jansen & Franz (2015): (1) the intercoxal process is divided at the midpoint  
957 between the coxae, but has both the anterior and posterior processes extending completely between  
958 the procoxae and contiguous with each other; and (2) the male tergum VII is nearly 4× as long as  
959 broad, respectively. In addition, the *M. gravivultus*-*M. griseus* [JF2015] clade (bsv = 3, rfd = 60),  
960 as resolved in the current cladogram, is congruent with that of Jansen & Franz (2015).

961        3. *Minyomerus* [JF2018] is nested within a well-supported clade of Tanymercini [non-focal] (boot =  
962                  100). However, further work is needed to assess the phylogenetic relationships between all genera  
963                  presently assigned to the Tanymercini [non-focal] (Alonso-Zarazaga & Lyal 1999).

#### 964        **Intrageneric relationships**

965        Within *Minyomerus* [JF2018], beginning at the earliest-bifurcating node and proceeding towards the  
966                  leaves, the first major incongruence with *Minyomerus* [JF2015] is the placement of *M. imberbus* [JF2015].  
967        This species was sister to the *M. constrictus*–*M. laticeps* [JF2015] clade, which in turn was sister to the  
968                  *M. aeruballux*–*M. conicollis* clade [JF2015]. The present analysis places *M. imberbus* [JF2015] in a  
969                  clade with *M. sculptilis* [JF2018] (see **Placement of newly described species**). The *M. aeriballux*–*M.*  
970                  *imberbus* clade [JF2018] (bsv = 2, rfd = 50) is supported by three synapomorphies: (1) presence of a  
971                  transverse constriction across the posterior of the frons (char. 16: 1); (2) presence of a reduced tuft of  
972                  post-ocular vibrissae (char. 21: 1); and (3) a mesally obscure lamina of the spiculum ventrale in the  
973                  female (char. 35: 1).

974        We resolve *M. cracens* [JF2015] as sister to the *M. aeriballux*–*M. bulbifrons* [JF2018] clade, inclusively  
975                  supported by three synapomorphies: (1) presence of a strongly punctate sulcus posteriad of the nasal plate  
976                  (char. 14: 2); (2) presence of broad scales on the terminal funicular segment of the antennae (char. 19: 1);  
977                  and (3) absence of a medial, anteriorly-directed, sclerotized process on the coxites of the ovipositor (char.  
978                  40: 1).

979        The *M. aeriballux*–*M. bulbifrons* [JF2018] clade is weakly supported by a single synapomorphy: the  
980                  width of the connection between the apodemes of the aedeagal tegmen is narrower than the base of the  
981                  apodeme (char. 52: 1). Within this clade, the position of the *M. bulbifrons*–*M. caseyi* clade [JF2018] clade  
982                  as separate from, and sister to, the *M. aeriballux*–*M. ampullaceus* clade [JF2018], is supported by one  
983                  synapomorphy and one homoplasious character, namely: (1) presence of an anterior ventral flange on the  
984                  style of the spiculum gastrale (char. 44: 1 – synapomorphic), and (2) differentiation of the setae on the  
985                  lateral portion of the elytra and on the venter from the setae on the elytral disc (char. 3: 1 – homoplasious).

#### 986        **Placement of newly described species**

987        Clades within *Minyomerus* [JF2018] not addressed in the preceding section are identical in topology and  
988                  composition to those of *Minyomerus* [JF2015], except for the addition of newly described species. Here  
989                  we assess the phylogenetic placements of these species. We also discuss similarities in the biogeographic  
990                  range of each species, in relation to the putative sister taxa, based on the results of species distribution  
991                  modeling (see Figs. 35–38).

#### 992        ***Minyomerus sculptilis* [JF2018]**

993        *Minyomerus sculptilis* [JF2018] is inferred as sister to *M. imberbus* [JF2015]. The *M. imberbus*–*M.*  
994                  *sculptilis* clade [JF2018] (bsv = 3, rfd = 72) is supported by a single synapomorphy and two homoplasious  
995                  characters: (1) corpus of spermatheca sinuate (char. 32: 1 – synapomorphic); (2) lamina of spiculum  
996                  gastrale in male longer than broad and anteriorly extended along style (char. 45: 1 – homoplasious); and  
997                  (3) aedeagal pedon medially sclerotized along dorsum (char. 51: 1 – homoplasious). In addition to these  
998                  characters, *M. imberbus* [JF2015] and *M. sculptilis* [JF2018] share a general external gestalt, which makes  
999                  separating these two species difficult, especially in damaged or worn specimens.

1000        Whereas *M. sculptilis* [JF2018] is associated with big sagebrush (*Artemisia tridentata* [non-focal]),  
1001                  tumbleweed (*Salsola tragus* [non-focal]), and tall tumblemustard (*Sisymbrium altissimum* [non-focal]);  
1002                  its sister taxon *M. imberbus* [JF2015] is associated with budsage (*Artemisia spinescens* [non-focal]).  
1003        The divergence of these two species may have been driven in part by differences in host-plant use.  
1004        However, this is less likely considering the generalist feeding habits of *Minyomerus* [JF2018] congeners.  
1005        Conversely, their divergence may have resulted from a vicariance event, based on their present-day  
1006                  biogeographic distributions, which are separated by the eastern extension of the Columbia Plateau.  
1007        *Minyomerus sculptilis* [JF2018] appears to be endemic to the Snake River Plain to the north, whereas *M.*  
1008                  *imberbus* [JF2015] has been found in the Great Basin Desert to the south.

#### 1009        ***Minyomerus tylotos* [JF2018]**

1010        *Minyomerus tylotos* [JF2018] is sister to *M. microps* [JF2015]. The *M. microps*–*M. tylotos* clade [JF2018]  
1011                  (bsv = 3, rfd = 73) is supported by a single synapomorphy and a single homoplasious character: (1) elytra  
1012                  and pronotum generally large, protuberant, and sculpted in appearance along dorsal and lateral faces (char.

1013 5: 1 – synapomorphic); and (2) sulcus posteriad of nasal plate broad and weakly punctate (char. 13: 1 –  
1014 homoplasious). In addition to these characters, the two species share a similar gestalt and uniform setation.

1015 *Minyomerus tylotos* [JF2018] appears to be endemic to northern Chihuahuan Desert, whereas *M.*  
1016 *microps* [JF2015] is widely distributed to the north throughout the Great Plains and along the Missouri  
1017 River. We consider it likely that *M. microps* [JF2015] represents a northern radiation of the common  
1018 ancestor of this clade. Conversely, *M. tylotos* [JF2018] may represent the ancestral distribution to the  
1019 south, based on the hypothesized origin of *Minyomerus* [JF2018] in the Chihuahuan Desert; see Jansen &  
1020 Franz (2015) and Wilson & Pitts 2010.

#### 1021 ***Minyomerus ampullaceus* [JF2018]**

1022 *Minyomerus ampullaceus* [JF2018] is sister to the *M. aeriballux*–*M. reburrus* clade [JF2015]. The *M.*  
1023 *aeriballux*–*M. ampullaceus* clade [JF2018] (bsv = 1, rfd = 50) is supported by a single synapomorphy:  
1024 lamina of spiculum ventrale with laminar arms basally bifurcating and sub-parallel mesally thereafter  
1025 (char. 37: 1). The placement of this species is tentative and based on the characteristics of a single, worn  
1026 specimen.

1027 Nonetheless, the biogeographic distributions of the species in the *M. aeriballux*–*M. ampullaceus*  
1028 clade [JF2018] exhibit overlap. *Minyomerus ampullaceus* [JF2018] is documented from Carlsbad, New  
1029 Mexico, in the western parts of the distributions of *M. aeriballux* [JF2015] and *M. reburrus* [JF2015].  
1030 The divergence of the latter two species is thought to be a result of their habitat and host plant preference,  
1031 given their overlapping ranges. *Minyomerus aeriballux* [JF2015] is found in very sandy soils and on  
1032 dune systems, whereas *M. reburrus* [JF2015] prefers arid grasslands. Without additional distributional or  
1033 host plant data for *M. ampullaceus* [JF2018], we cannot assess whether the single documented locality  
1034 for this species represents the center or edge of its range. However, this locality does overlap with the  
1035 known range of its sister clade, suggesting that the divergence of *M. ampullaceus* [JF2018] from the *M.*  
1036 *aeriballux*–*M. ampullaceus* clade [JF2018] was not a vicariance event.

#### 1037 ***Minyomerus franko* [JF2018]**

1038 *Minyomerus franko* [JF2018] is sister to the *M. caseyi*–*M. trisetosus* clade [JF2015]. The *M. caseyi*–*M.*  
1039 *franko* clade [JF2018] (bsv = 4, rfd = 63) is supported by a single synapomorphy and two homoplasious  
1040 characters: (1) rows of setae on elytral intervals comprised of larger white setae randomly interspersed  
1041 among smaller brown setae(char. 4: 1 – synapomorphic); (2) prementum lacking strong ligula and  
1042 straight margins, not appearing pentagonal (char. 7: 0 – homoplasious); and (3) anterior margin of female  
1043 tergum VII entirely free of sclerotized band (char. 41: 1 – homoplasious). In addition to these characters,  
1044 members of this clade share a generally similar gestalt, especially regarding the head and rostrum, and the  
1045 articulation between the pronotum and elytra in dorsal and lateral view. The interspersed, white elytral  
1046 setae of these three species exhibit varying degrees of apical expansion, and can appear moderately to  
1047 greatly explanate or spatulate in at least some, but not all, specimens.

1048 *Minyomerus franko* [JF2018] has been documented on spear globemallow *Sphaeralcea hastulata*  
1049 [non-focal]. *Minyomerus trisetosus* [JF2015] is associated with broomweed *Xanthocephalum* [non-focal],  
1050 creosote bush *Larrea tridentata* [non-focal] and snakeweed *Gutierrezia* [non-focal]. *Minyomerus caseyi*  
1051 has no known plant associations. It is therefore possible that the divergence of *M. franko* [2018] was  
1052 facilitated by differences in host-plant preference. However, this remains unlikely given the generalist  
1053 feeding habits of congeners.

1054 Alternatively, the speciation sequence in the *M. caseyi*–*M. franko* clade [JF2018] may correspond to  
1055 vicariance events. *Minyomerus trisetosus* [JF2015] inhabits a broad swath of the northern Chihuahuan  
1056 Desert, whereas *M. franko* [JF2018] and *M. caseyi* [JF2015] are exclusively encountered in the southern  
1057 Chihuahuan Desert. MaxEnt predicts overlapping species distributions for the latter two species. However,  
1058 the *documented* localities of these two species pertain to distinct biogeographic regions. *Minyomerus*  
1059 *franko* [JF2018] has only been collected in the valleys of the Sierra Madre Oriental range, whereas  
1060 *M. caseyi* [JF2015] is found along the western edge of this range, in the eastern portion of the Central  
1061 Mexican Plateau. Additional occurrence records are needed to clarify the spatial extents of these species'  
1062 distributions, and thus draw more robust inferences regarding their endemism.

## 1063 CONCLUSIONS

1064 Through addition of four herein described species, the entimine [non-focal] genus *Minyomerus* [JF2018]  
1065 is expanded to include 21 species. We predict that additional undescribed species of *Minyomerus* [JF2018]

1066 exist throughout the North American deserts, given the narrow endemicity patterns of many members  
1067 of the genus. Furthermore, we believe that sampling in poorly-sampled locales, particularly in the  
1068 northwestern United States and in northern Mexico, will yield new evolutionary insights for this group.  
1069 New molecular data can strengthen phylogenetic hypotheses and provide estimates regarding the timing  
1070 of diversification of *Minyomerus* [JF2018], thereby testing our current inference of an origin in central  
1071 Mexico. Another research direction should focus on the reproductive behavior of certain species suspected  
1072 to be parthenogenetic; including rearing and karyotyping. Finally, the validity of the genus *Minyomerus*  
1073 [JF2018] as a member of the Tanytarsiini [non-focal], and its relationships to other Entiminae [non-focal],  
1074 remain uncertain.

## 1075 ACKNOWLEDGMENTS

1076 The authors are grateful to Robert Anderson (CMNC), Ed Riley and John Oswald (TAMU), and Lourdes  
1077 Chamorro (USNM) for their assistance and provision of specimens used in this ~~revision study~~. The authors  
1078 also thank Salvatore Anzaldo, Andrew Johnston, Sangmi Lee and other ASUHIC members for their  
1079 assistance in procuring, treating, and maintaining specimen loans upon entry into the ASUHIC. ~~This~~  
1080 ~~research was funded in part by the National Science Foundation (DEB-1155984) and the United States~~  
1081 ~~Department of Agriculture—Agricultural Research Service (Agreement 58-1275-1-335).~~

## 1082 SUPPLEMENTAL INFORMATION

1083 **SI1** Explanation of the RCC–5 alignment approach. File format: .pdf  
1084 **SI2A** Input constraints for the *Minyomerus* [JF2018]/[JF2015] rank-only classification alignment. File  
1085 format: .txt  
1086 **SI2B** Input visualization for the SI2A input. File format: .pdf  
1087 **SI2C** Set of 114 *Maximally Informative Relations* (MIR) for the SI2A input. File format: .csv  
1088 **SI2D** Alignment visualization for the SI2A input. File format: .pdf  
1089 **SI3A** Input constraints for the *Minyomerus* [JF2018]/[JF2015] phylogeny alignment – whole-concept  
1090 resolution with overlap. File format: .txt  
1091 **SI3B** Input visualization for the SI3A input. File format: .pdf  
1092 **SI3C** Set of 925 *Maximally Informative Relations* (MIR) for the SI3A input. File format: .csv  
1093 **SI3D** Alignment visualization for the SI3A input. File format: .pdf  
1094 **SI4A** Input constraints for the *Minyomerus* [JF2018]/[JF2015] phylogeny alignment – split-concept  
1095 resolution. File format: .txt  
1096 **SI4B** Input visualization for the SI4A input. File format: .pdf  
1097 **SI4C** Set of 925 *Maximally Informative Relations* (MIR) for the SI4A input. File format: .csv  
1098 **SI4D** Alignment visualization for the SI4A input. File format: .pdf

## 1099 FUNDING STATEMENT

1100 ~~This research was funded in part by the National Science Foundation (DEB-1155984) and the United~~  
1101 ~~States Department of Agriculture—Agricultural Research Service (Agreement 58-1275-1-335). There~~  
1102 ~~was no additional external funding received for this study.~~

1103 **REFERENCES**

- 1104 Agnarsson, I. & Miller, J. A. (2008), 'Is ACCTRAN better than DELTRAN?', *Cladistics* **24**(6), 1032–  
1105 1038.
- 1106 Alonso-Zarazaga, M. A. & Lyal, C. H. C. (1999), *A world catalogue of families and genera of Cur-*  
1107 *culionoidea (Insecta: Coleoptera)*, Entomopraxis, Barcelona, Spain.
- 1108 Anderson, R. S. (2002), Curculionidae, in R. H. Arnett Jr., M. C. Thomas, P. E. Skelley & J. H. Frank,  
1109 eds, 'American Beetles, Volume 2, Polyphaga: Scarabaeoidea to Curculionoidea', CRC Press, Boca  
1110 Raton, FL, chapter 131, p. 722–815.
- 1111 Arnett Jr., R. H., Samuelson, G. A., Nishida, G. M. et al. (1993), *The insect and spider collections of the*  
1112 *world*., 2 edn, Sandhill Crane Press, Inc., Gainesville, Florida.
- 1113 Blackwelder, R. E. & Blackwelder, R. M. (1948), *Fifth Supplement, 1939 to 1947 (Inclusive) to the Leng*  
1114 *Catalogue of Coleoptera of America, North of Mexico*, Mount Vernon, Virginia.
- 1115 Boheman, C. H. (1833), 12. T. Microsus, in C. J. Schoenherr, ed., 'Genera et species curculionidum, cum  
1116 synonymia hujus familiae', Vol. 1:2, Nicolas-Edme Roret, Paris, France, pp. 523–524.
- 1117 Bouchard, P., Bousquet, Y., Davies, A. E., Alonso-Zarazaga, M. A., Lawrence, J. F., Lyal, C. H., Newton,  
1118 A. F., Reid, C. A., Schmitt, M., Ślipiński, S. A. et al. (2011), 'Family-group names in Coleoptera  
1119 (Insecta)', *ZooKeys* **88**, 1–972.
- 1120 Bremer, K. A. et al. (1994), 'Branch support and tree stability', *Cladistics* **10**(3), 295–304.
- 1121 Brown, R. W. (1956), *Composition of scientific words*, Smithsonian Institution Press, Washington, DC.
- 1122 Casey, T. L. (1889), 'On some new north american rhynchophora', *Annals of the New York Academy of*  
1123 *Sciences* **4**(1), 229–296.
- 1124 Chen, M., Yu, S., Franz, N., Bowers, S. & Ludäscher, B. (2014), 'Euler/x: A toolkit for logic-based  
1125 taxonomy integration', *arXiv* **1402**(1992), 1–8.
- 1126 de la Torre-Bueno, J. R., Nichols, S. W., Tulloch, G. S., de la Torre-Bueno, J. R. et al. (1989), *Torre-Bueno*  
1127 *glossary of entomology*, New York Entomological Society in cooperation with the American Museum  
1128 of Natural History, New York City, New York.
- 1129 Elith, J., Phillips, S. J., Hastie, T., Dudík, M., Chee, Y. E. & Yates, C. J. (2011), 'A statistical explanation  
1130 of MaxEnt for ecologists', *Diversity and distributions* **17**(1), 43–57.
- 1131 Farris, J. S. (1989), 'The retention index and the rescaled consistency index', *Cladistics* **5**(4), 417–419.
- 1132 Franz, N. M. (2010a), 'Redescriptions of critical type species in the *Eustylini* Lacordaire (Coleoptera:  
1133 Curculionidae: Entiminae)', *Journal of Natural History* **44**(1–2), 41–80.
- 1134 Franz, N. M. (2010b), 'Revision and phylogeny of the Caribbean weevil genus *Apotomoderes* Dejean,  
1135 1834 (Coleoptera, Curculionidae, Entiminae).', *ZooKeys* **49**.
- 1136 Franz, N. M. (2012), 'Phylogenetic reassessment of the *Exophthalmus* genus complex (Curculionidae:  
1137 Entiminae: Eustylini, Geonemini)', *Zoological Journal of the Linnean Society* **164**(3), 510–557.
- 1138 Franz, N. M. (2014), 'Anatomy of a cladistic analysis', *Cladistics* **30**(3), 294–321.
- 1139 Franz, N. M., Chen, M., Kianmajd, P., Yu, S., Bowers, S., Weakley, A. S. & Ludäscher, B. (2016b),  
1140 'Names are not good enough: Reasoning over taxonomic change in the andropogon complex', *Semantic*  
1141 *Web (IOS)* **7**(6), 645–667.
- 1142 Franz, N. M., Musher, L. J., Brown, J. W., Yu, S., hen, M., Yu, S. & Ludäscher, B. (2018), 'Verbalizing  
1143 phylogenomic conflict: Representation of node congruence across competing reconstructions of the  
1144 neoavian explosion', *bioRxiv* pp. 1–52. <https://doi.org/10.1101/233973>.
- 1145 Franz, N. M. & Peet, R. K. (2009), 'Towards a language for mapping relationships among taxonomic  
1146 concepts', *Systematics and Biodiversity* **7**(1), 5–20.
- 1147 Franz, N. M., Pier, N. M., Reeder, D. M., Chen, M., Yu, S., Kianmajd, P., Bowers, S. & Ludäscher, B.  
1148 (2016a), 'Two influential primate classifications logically aligned', *Systematic Biology* **65**(4), 561–582.
- 1149 Goloboff, P. A. (1999), *NONA - Version 2.0 (for Windows)*. <http://www.cladistics.com>.
- 1150 Goloboff, P. A. & Farris, J. S. (2001), 'Methods for quick consensus estimation', *Cladistics* **17**(1), S26–  
1151 S34.
- 1152 Goloboff, P. A., Farris, J. S. & Nixon, K. C. (2008), 'Tnt, a free program for phylogenetic analysis',  
1153 *Cladistics* **24**(5), 774–786.
- 1154 Google Inc. (2018), *Google Earth Pro - Version 7.3.1.4507*. <https://www.google.com/earth/>.
- 1155 Green, J. W. (1920), 'Notes on American Rhynchophora (Col.)', *Entomological News* **31**, 193–201.
- 1156 Hijmans, R. J., Cameron, S. E., Parra, J. L., Jones, P. G. & Jarvis, A. (2005), 'Very high resolution  
1157 interpolated climate surfaces for global land areas', *International journal of climatology* **25**(15), 1965–

- 1158 1978.
- 1159 Hijmans, R. J., Garcia, N., Kapoor, J., Rala, A., Maunahan, A. & Wieczorek, J. (2012), *Global administrative areas (boundaries)*, Museum of Vertebrate Zoology and the International Rice Research Institute, University of California, Berkeley, California. <http://www.gadm.org/>.
- 1160
- 1161
- 1162 Horn, G. H. (1876), Family V. OTIORHYNCHIDÆ, in J. L. LeConte & G. H. Horn, eds, 'The Rhynchophora of America, north of Mexico', Vol. 15, Proceedings of the American Philosophical Society, New York City, New York, pp. 13–112.
- 1163
- 1164
- 1165 Howden, A. T. (1959), 'A revision of the species of *Pandeleteius* Schönherr and *Pandeleteinus* Champion of America north of Mexico: (Coleoptera: Curculionidae)', *Proceedings of the California Academy of Sciences* **29**, 361–421.
- 1166
- 1167
- 1168 Howden, A. T. (1970), 'The Tanymecini of the West Indies (Coleoptera: Curculionidae)', *Contributions of the American Entomological Institute* **5**, 1–73.
- 1169
- 1170 Howden, A. T. (1982), 'Revision of the New World genus *Hadromeropsis* Pierce (Coleoptera, Curculionidae, Tanymecini)', *Contributions of the American Entomological Institute* **19**, 1–180.
- 1171
- 1172 Howden, A. T. (1995), 'Structures related to oviposition in Curculionoidea', *Memoirs of the Entomological Society of Washington* **14**, 53–100.
- 1173
- 1174 Jansen, M. A. & Franz, N. M. (2015), 'Phylogenetic revision of *Minyomerus* Horn, 1876 sec. Jansen and Franz, 2015 (Coleoptera: Curculionidae) using taxonomic concept annotations and alignments', *ZooKeys* **528**, 1–133.
- 1175
- 1176
- 1177 Kissinger, D. G. (1964), *Curculionidae of America North of Mexico. A Key to the Genera*, Taxonomic Publications, South Lancaster, Massachusetts.
- 1178
- 1179 LeConte, J. L. (1859), *The Complete Writings of Thomas Say on the Entomology of North America*, Baillière Brothers, London, England.
- 1180
- 1181 LeConte, J. L. & Horn, G. H. (1876), 'The Rhynchophora of America, north of Mexico', *Proceedings of the American Philosophical Society* **15**(96), 1–455.
- 1182
- 1183 Marvaldi, A. E. (1997), 'Higher level phylogeny of Curculionidae (Coleoptera: Curculionoidea) based mainly on larval characters, with special reference to broad-nosed weevils', *Cladistics* **13**(4), 285–312.
- 1184
- 1185 Marvaldi, A. E., Lanteri, A. A., del Río, M. G. & Oberprieler, R. G. (2014), Entiminae Schoenherr, 1823, in R. A. B. Leschen & R. G. Beutel, eds, 'Handbook of Zoology: Arthropoda: Insecta: Coleoptera Volume 3: Morphology and Systematics (Phytophaga)', De Gruyter, Berlin, Germany, chapter 3.7.5, p. 503–522.
- 1186
- 1187
- 1188
- 1189 Morimoto, K. & Kojima, H. (2003), 'Morphologic characters of the weevil head and phylogenetic implications (Coleoptera, Curculionoidea)', *Esakia* **43**, 133–169.
- 1190
- 1191 Munz, P. A. & Keck, D. D. (1973), *A Californian flora (with supplement)*, University of California Press, Berkeley, California.
- 1192
- 1193 Nixon, K. C. & Carpenter, J. M. (1993), 'On outgroups', *Cladistics* **9**(4), 413–426.
- 1194 Nixon, K. C. et al. (2002), *WinClada - Version 1.00. 08*. <http://www.diversityoflife.org/winclada/>.
- 1195 Oberprieler, R. G., Anderson, R. S. & Marvaldi, A. E. (2014), Curculionoidea Latreille, 1802: Introduction, Phylogeny, in R. A. B. Leschen & R. G. Beutel, eds, 'Handbook of Zoology: Arthropoda: Insecta: Coleoptera Volume 3: Morphology and Systematics (Phytophaga)', De Gruyter, Berlin, Germany, chapter 3, pp. 285–300.
- 1196
- 1197
- 1198
- 1199 Oberprieler, R. G., Marvaldi, A. E. & Anderson, R. S. (2007), 'Weevils, weevils, weevils everywhere', *Zootaxa* **1668**(1), 491–520.
- 1200
- 1201 O'Brien, C. W. & Wibmer, G. J. (1982), *Annotated checklist of the weevils (Curculionidae sensu lato) of North America, Central America, and the West Indies (Coleoptera: Curculionoidea)*, American Entomological Institute, Ann Arbor, Michigan.
- 1202
- 1203
- 1204 Phillips, S. J., Anderson, R. P. & Schapire, R. E. (2006), 'Maximum entropy modeling of species geographic distributions', *Ecological modelling* **190**(3–4), 231–259.
- 1205
- 1206 Phillips, S. J., Dudík, M. & Schapire, R. E. (2004), A maximum entropy approach to species distribution modeling, in 'Proceedings of the 21st International Conference on Machine Learning', ACM, pp. 83–90.
- 1207
- 1208 Pierce, W. D. (1909), 'Studies of North American weevils', *Proceedings of the United States National Museum* **37**(1708), 325–364.
- 1209
- 1210 Pierce, W. D. (1913), 'Miscellaneous contributions to the knowledge of the weevils of the families Attelabidae and Brachyrhinidae', *Proceedings of the United States National Museum* **45**(1988), 365–426.
- 1211
- 1212

- 1213 Quantum GIS Development Team (2018), ‘Quantum GIS Geographic Information System’, *Open Source*  
1214 *Geospatial Foundation Project*. <http://qgis.osgeo.org>.
- 1215 Rieppel, O. (2007), ‘The performance of morphological characters in broad-scale phylogenetic analyses’,  
1216 *Biological Journal of the Linnean Society* **92**(2), 297–308.
- 1217 Say, T. (1831), Descriptions of North American Curculionides and an arrangement of some of our known  
1218 species agreeably to the method of Schoenherr, *in* J. L. LeConte, ed., ‘The Complete Writings of  
1219 Thomas Say on the Entomology of North America’, Vol. 1, Baillière Brothers, London, England,  
1220 pp. 1–30.
- 1221 SEINet (2018), *Southwest Environmental Information Network*. <http://swbiodiversity.org/seinet/index.php>.
- 1222 Sharp, D. (1891), Coleoptera. Rhynchophora. Curculionidae. Attelabinae, Pterocolinae, Allocoryninae,  
1223 Apioninae, Thecesterninae, Otiorhynchinae [part, “Apterae”], *in* D. Sharp & G. C. Champion, eds,  
1224 ‘Biologia Centrali-Americanana’, Vol. 4:3, London, England, pp. 87–177.
- 1225 Sleeper, E. L. (1960), ‘Notes on the Curculionoidea II: 20. a contribution to the knowledge of the  
1226 Curculionoidea’, *Ohio Journal of Science* **60**(2), 83–88.
- 1227 Thompson, R. T. (1992), ‘Observations on the morphology and classification of weevils (Coleoptera,  
1228 Curculionoidea) with a key to major groups’, *Journal of Natural History* **26**(4), 835–891.
- 1229 Ting, P. C. (1936), ‘The mouth parts of the coleopterous group Rhynchophora’, *Microentomology*  
1230 **1**, 93–114.
- 1231 Wheeler, Q. D. & Platnick, N. I. (2000), The phylogenetic species concept (*sensu* Wheeler and Platnick),  
1232 *in* Q. D. Wheeler & R. Meier, eds, ‘Species Concepts and Phylogenetic Theory: a Debate’, Columbia  
1233 University Press, New York City, New York, pp. 55–69.
- 1234 Wilson, J. S. & Pitts, J. P. (2010), ‘Illuminating the lack of consensus among descriptions of earth  
1235 history data in the north american deserts: a resource for biologists’, *Progress in Physical Geography*  
1236 **34**(4), 419–441.



**Figure 1. Dorsal habitus of *M. ampullaceus* [JF2018].** Image of female (♀) holotype.



**Figure 2.** Lateral habitus of *M. ampullaceus* [JF2018]. Image of female (♀) holotype.



**Figure 3.** Ventral habitus of *M. ampullaceus* [JF2018]. Image of female (♀) holotype.



**Figure 4.** Head and rostrum of *M. ampullaceus* [JF2018]. Frontal view of female (♀) holotype.



**Figure 5.** Spermatheca of *M. ampullaceus* [JF2018]. Genitalia of female (♀) holotype.



**Figure 6.** Lamina of spiculum ventrale of *M. ampullaceus* [JF2018]. Sternum VIII of female (♀) holotype.



**Figure 7.** Dorsal habitus of *M. franko* [JF2018]. Image of female (♀) holotype.



**Figure 8.** Lateral habitus of *M. franko* [JF2018]. Image of female (♀) holotype.



**Figure 9.** Ventral habitus of *M. franko* [JF2018]. Image of female (♀) holotype.



**Figure 10. Head and rostrum of *M. franko* [JF2018].** Frontal view of female (♀) holotype.



**Figure 11.** Maxilla of *M. franko* [JF2018]. Dextral maxilla of female ( $\text{♀}$ ) paratype.



**Figure 12.** Prementum of *M. franko* [JF2018]. Labium of female (♀) paratype.



**Figure 13.** Spermatheca of *M. franko* [JF2018]. Genitalia of female (♀) paratype.

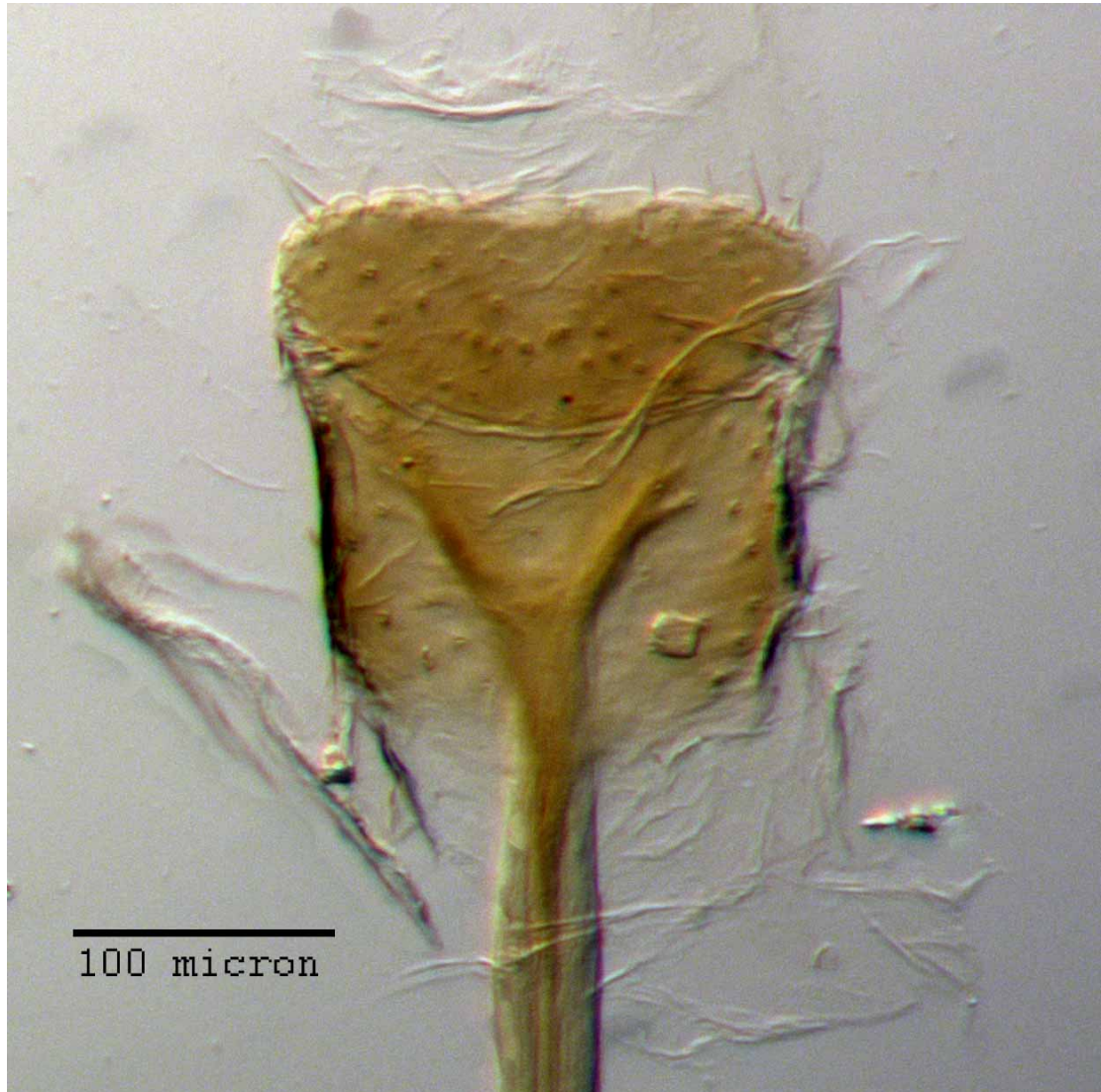


**Figure 14.** Lamina of spiculum ventrale of *M. franko* [JF2018]. Sternum VIII of female (♀) paratype.



**Figure 15. Aedeagus of *M. franko* [JF2018].** Genitalia of male ( $\sigma$ ) paratype in (A) dorsal view and (B) lateral view.



**Figure 16.** Dorsal habitus of *M. sculptilis* [JF2018]. Image of female (♀) holotype.



**Figure 17.** Lateral habitus of *M. sculptilis* [JF2018]. Image of female (♀) holotype.



**Figure 18.** Ventral habitus of *M. sculptilis* [JF2018]. Image of female (♀) holotype.



**Figure 19. Head and rostrum of *M. sculptilis* [JF2018].** Frontal view of female (♀) holotype.

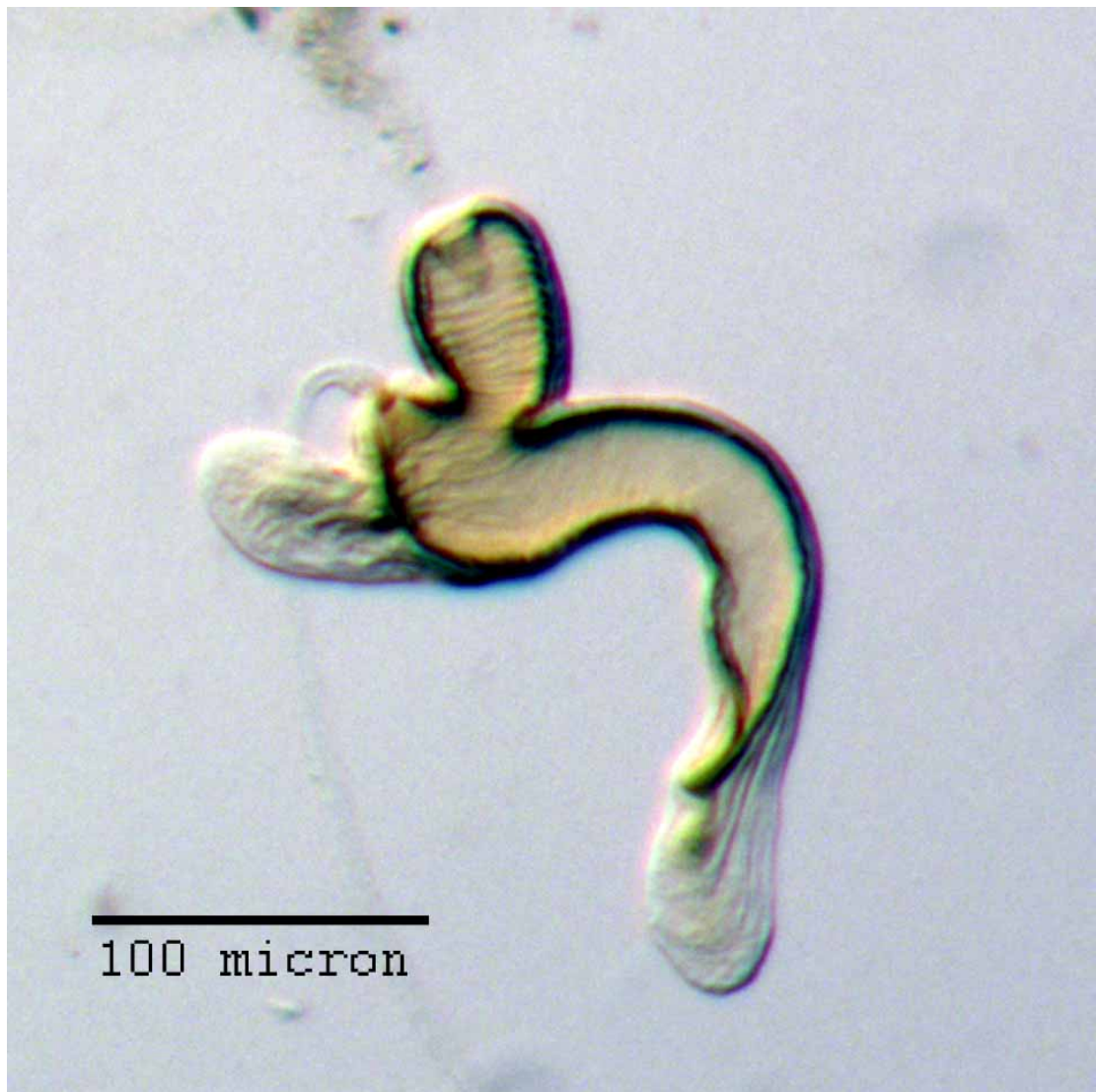


**Figure 20.** Spermatheca of *M. sculptilis* [JF2018]. Genitalia of female (♀) paratype.

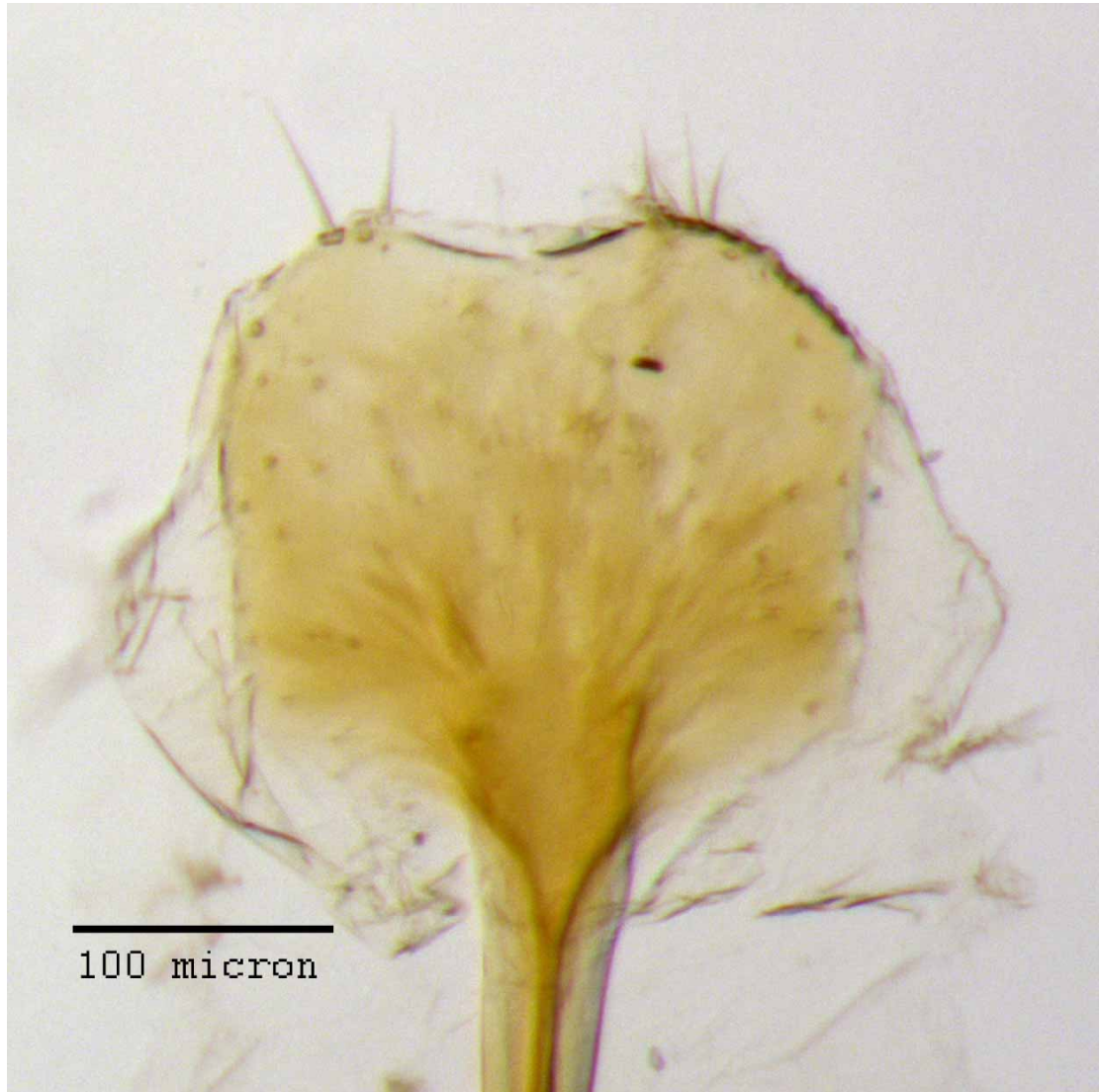


**Figure 21.** Lamina of spiculum ventrale of *M. sculptilis* [JF2018]. Sternum VIII of female (♀) paratype.



**Figure 22. Aedeagus of *M. sculptilis* [JF2018].** Genitalia of male ( $\sigma$ ) paratype in (A) dorsal view and (B) lateral view.



**Figure 23.** Dorsal habitus of *M. tylotos* [JF2018]. Image of female (♀) holotype.



**Figure 24.** Lateral habitus of *M. tylotos* [JF2018]. Image of female (♀) holotype.



**Figure 25.** Ventral habitus of *M. tylotos* [JF2018]. Image of female (♀) holotype.



**Figure 26. Head and rostrum of *M. tylotos* [JF2018].** Frontal view of female (♀) holotype.

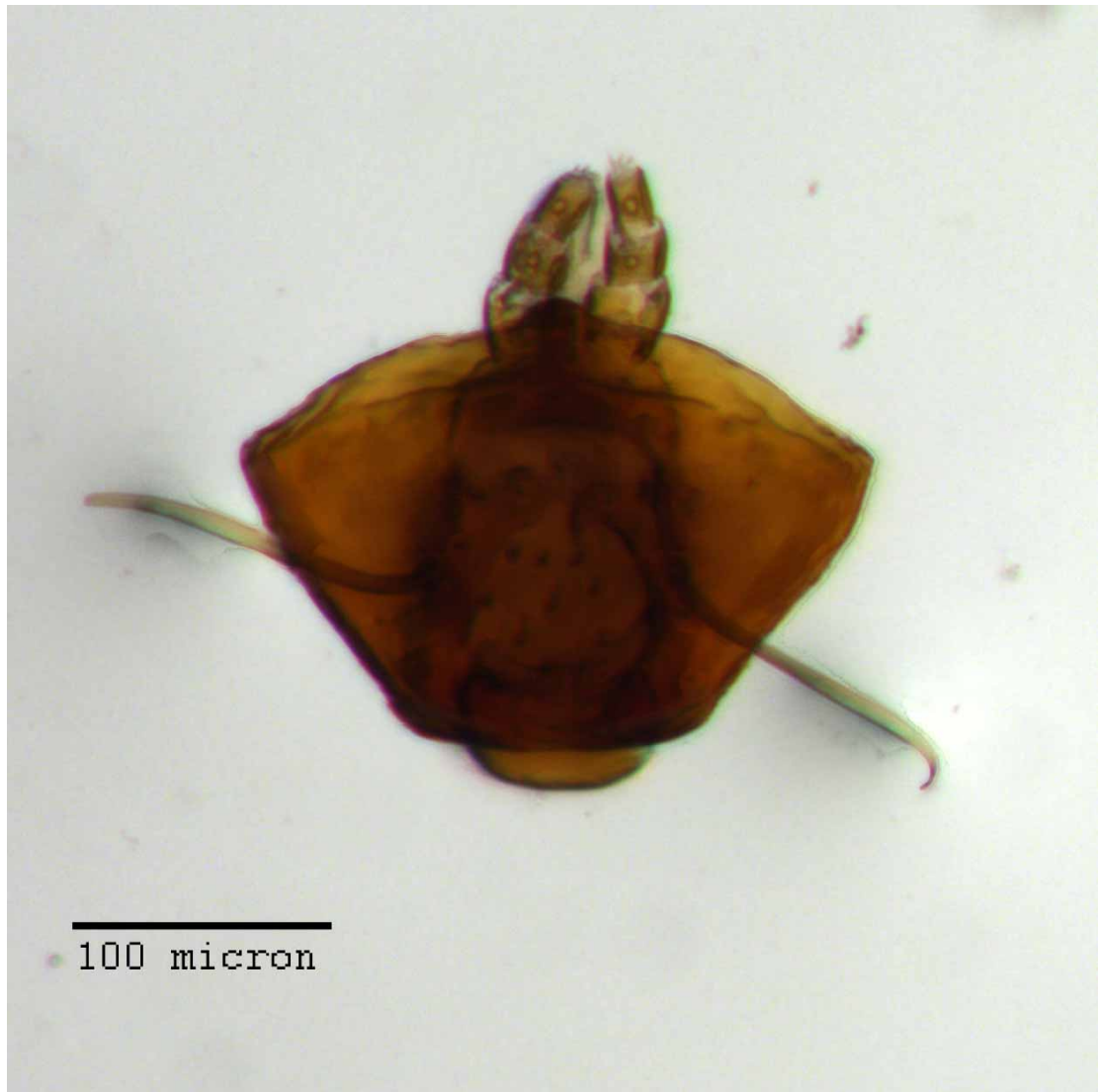


**Figure 27.** Prementum of *M. tylotos* [JF2018]. Labium of female (♀) paratype.



**Figure 28.** Spermatheca of *M. tylotos* [JF2018]. Genitalia of female (♀) paratype.



**Figure 29.** Lamina of spiculum ventrale of *M. tylotos* [JF2018]. Sternum VIII of female (♀) paratype.

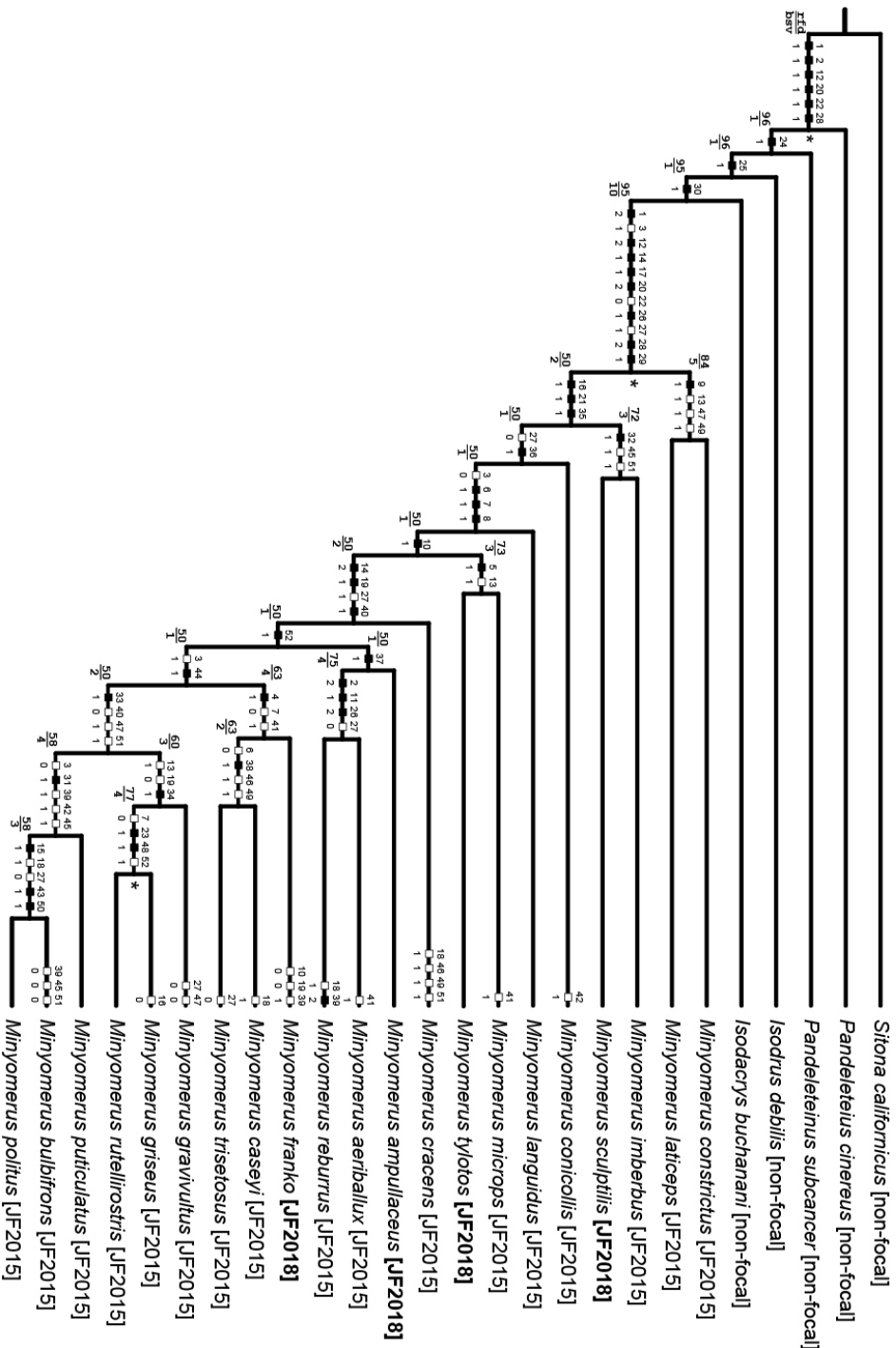


**Figure 30. Preferred phylogeny – character transitions and support.** Single most parsimonious cladogram representing the preferred phylogeny of species of *Minyomerus* [JF2018], and select outgroup taxa ( $L = 99$ ,  $CI = 60$ ,  $RI = 80$ ). Characters 9, 27, 39, 45 - 47, 49, and 51 are mapped under ACCTRAN optimization; all others are unambiguously optimized. Black squares indicate non-homoplasious character state changes, whereas white squares indicate homoplasious character state changes. The numbers above and below the squares represent character numbers and states, respectively. Bremer support (upper value) and relative fit difference (lower value) values can be found at the left ends of the branches. A "\*" symbol at the right end of a branch indicates Bootstrap support greater than 0.95.

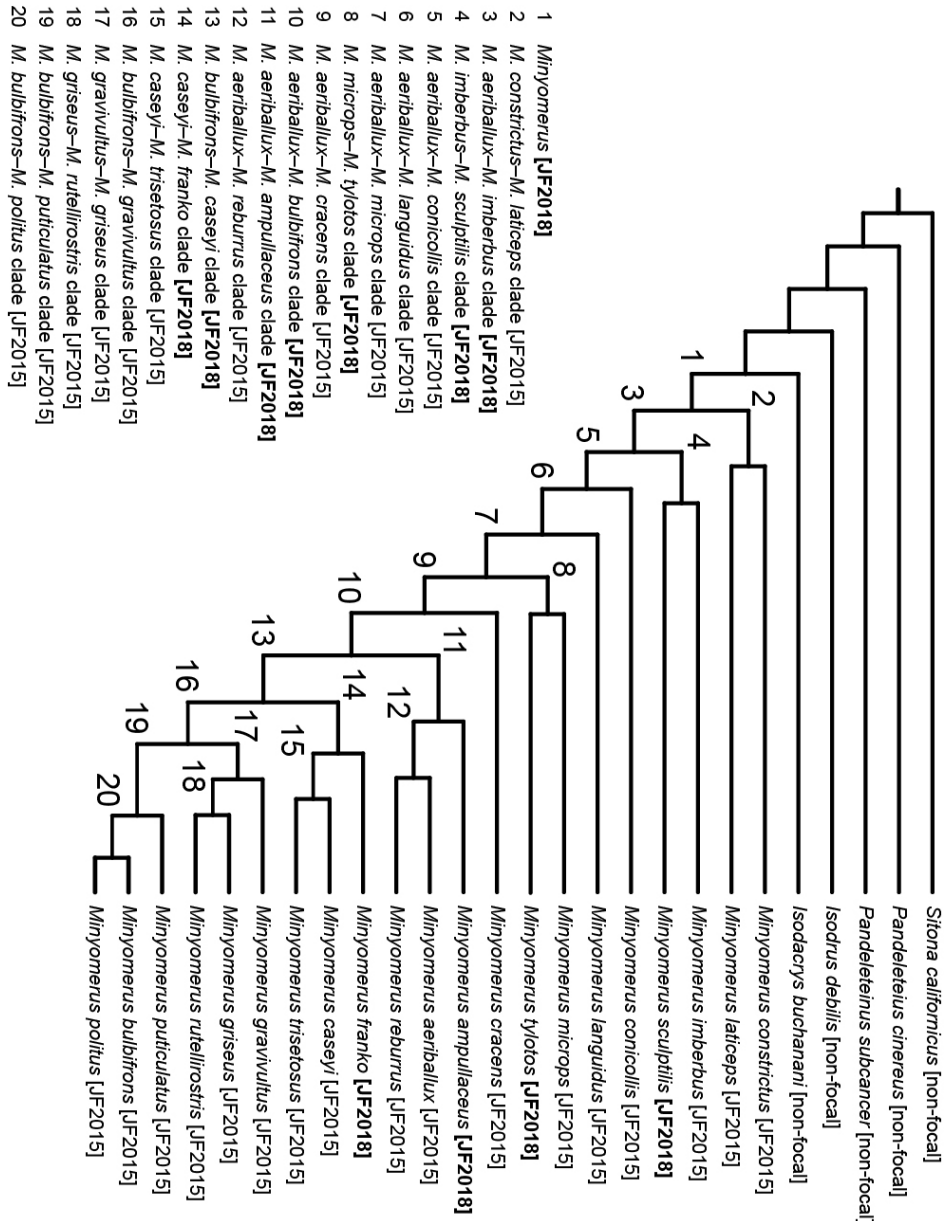


**Figure 31. Preferred phylogeny – clade concept labels.** Topology and species-level taxonomic concept labels as in Fig. 30. Clade concept labels, numbered 1-20, are consistently generated by using the alphabetically first epithet in each of the bifurcating sister clades. This method safeguards the clade concept labels against changes due simply to reorientation of leaves. Bold-font square brackets indicate new [JF2018] labels. See also **RCC-5 Alignments**.

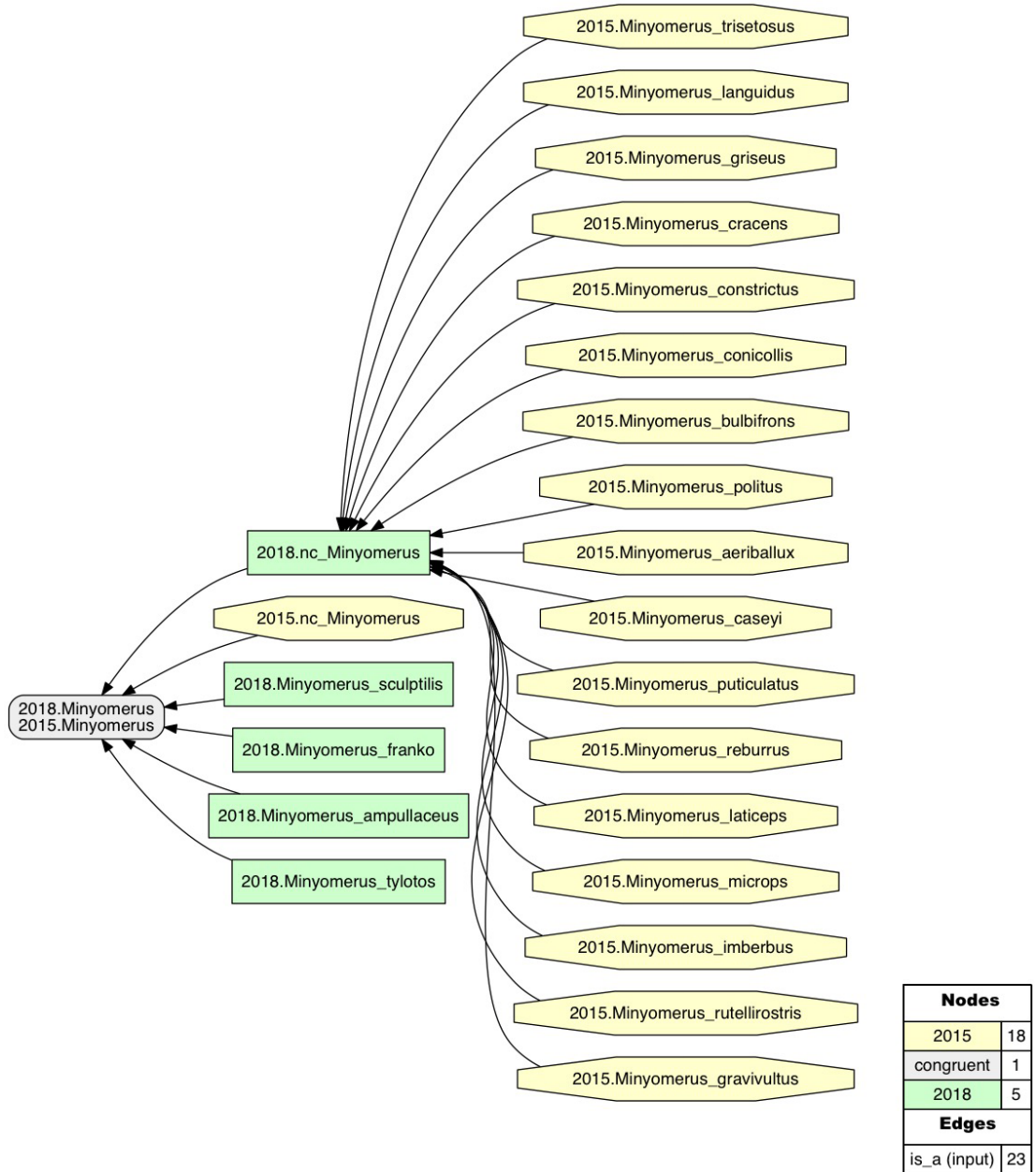


**Figure 32. Intensional RCC-5 alignment of the rank-only classifications of *Minyomerus* [JF2018]/[JF2015].** See also Jansen & Franz (2015) and Supplemental Information SI2. Taxonomic concept labels such as *Minyomerus microps* [JF2015] are abbreviated as "2015.Minyomerus\_microps". Relaxation of the coverage constraint is indicated with the prefix "nc\_" (no coverage). Congruent concept regions ( $T_2$  and  $T_1$ ) are shown as grey rectangles, concepts regions unique to the later taxonomy ( $T_2$ ) are shown as green rectangles, and concept regions unique to the earlier taxonomy ( $T_1$ ) are shown as yellow octagons. Articulations of inverse proper inclusion ( $<$ ) and overlap ( $><$ ), where present, are also shown.

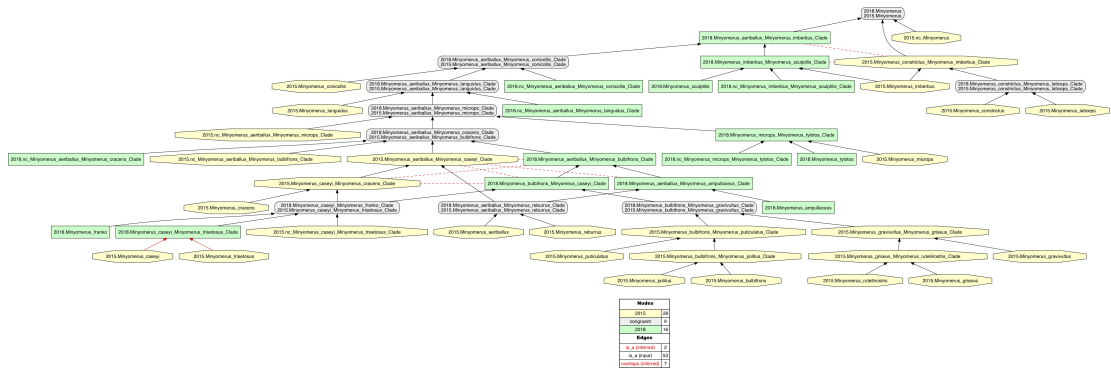


**Figure 33. Intensional RCC–5 alignment of the phylogenies of *Minyomerus* [JF2018]/[JF2015] – whole-concept resolution with overlap.** See also **Supplemental Information SI3**. Seven overlapping articulations are inferred. For further discussion, see the **RCC–5 Alignments** section.

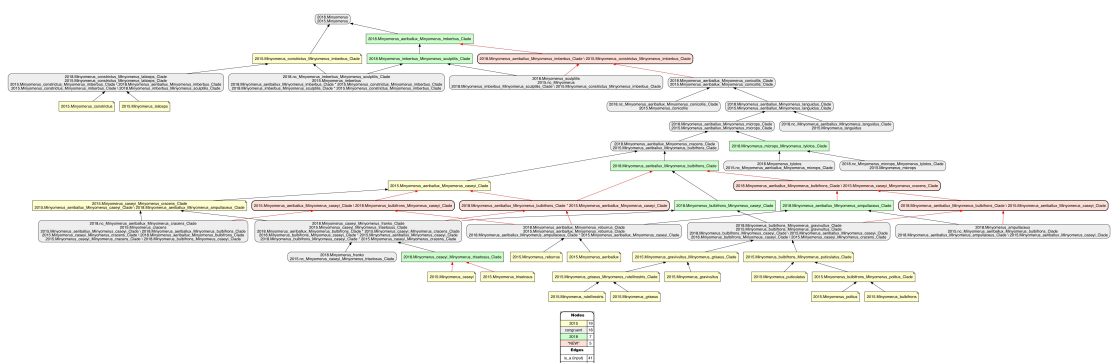


**Figure 34. Intensional RCC–5 alignment of the phylogenies of *Minyomerus* [JF2018]/[JF2015] – split-concept resolution.** See also **Supplemental Information SI4**. The seven overlapping articulations of the alignment displayed Fig. 33 are resolved into their constituent split regions. That is, if regions A and B overlap, the three resulting split regions are labeled A\|b ("A, not b"), A\*B ("A and B"), and B\|a ("B, not a"). Five split-concept regions can *only* be named using this convention, and are salmon-colored in the alignment visualization.

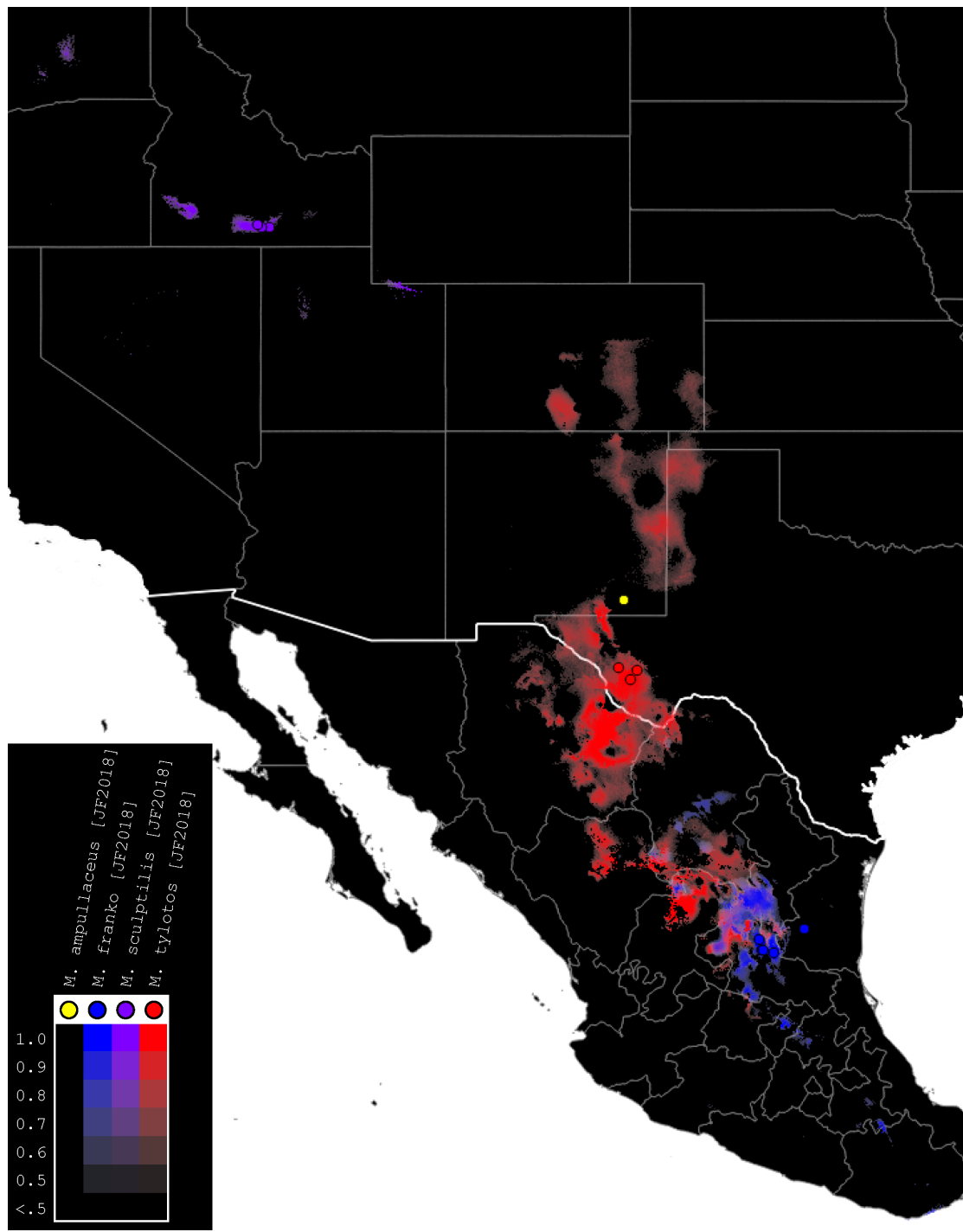


**Figure 35. Summary map of distributions of new species of *Minyomerus* [JF2018].** Combined occurrence record and Maxent habitat modeling map for four newly-described species of *Minyomerus* [JF2018], as indicated in the legend.

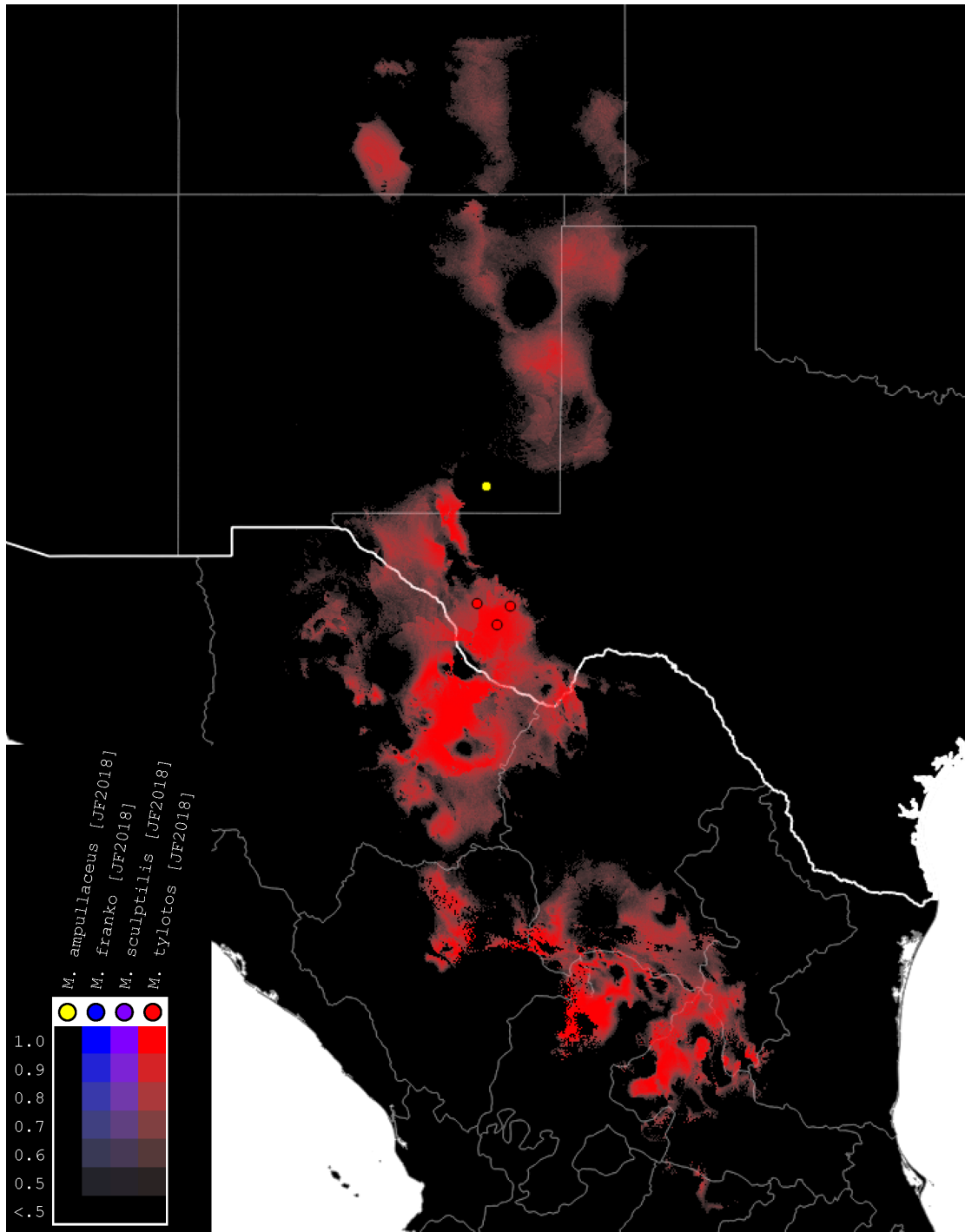


**Figure 36. Distributions of *M. ampullaceus* [JF2018] and *M. tylotos* [JF2018].** Combined occurrence record and Maxent habitat modeling map for *M. ampullaceus* [JF2018] and *M. tylotos* [JF2018], as indicated in the legend.

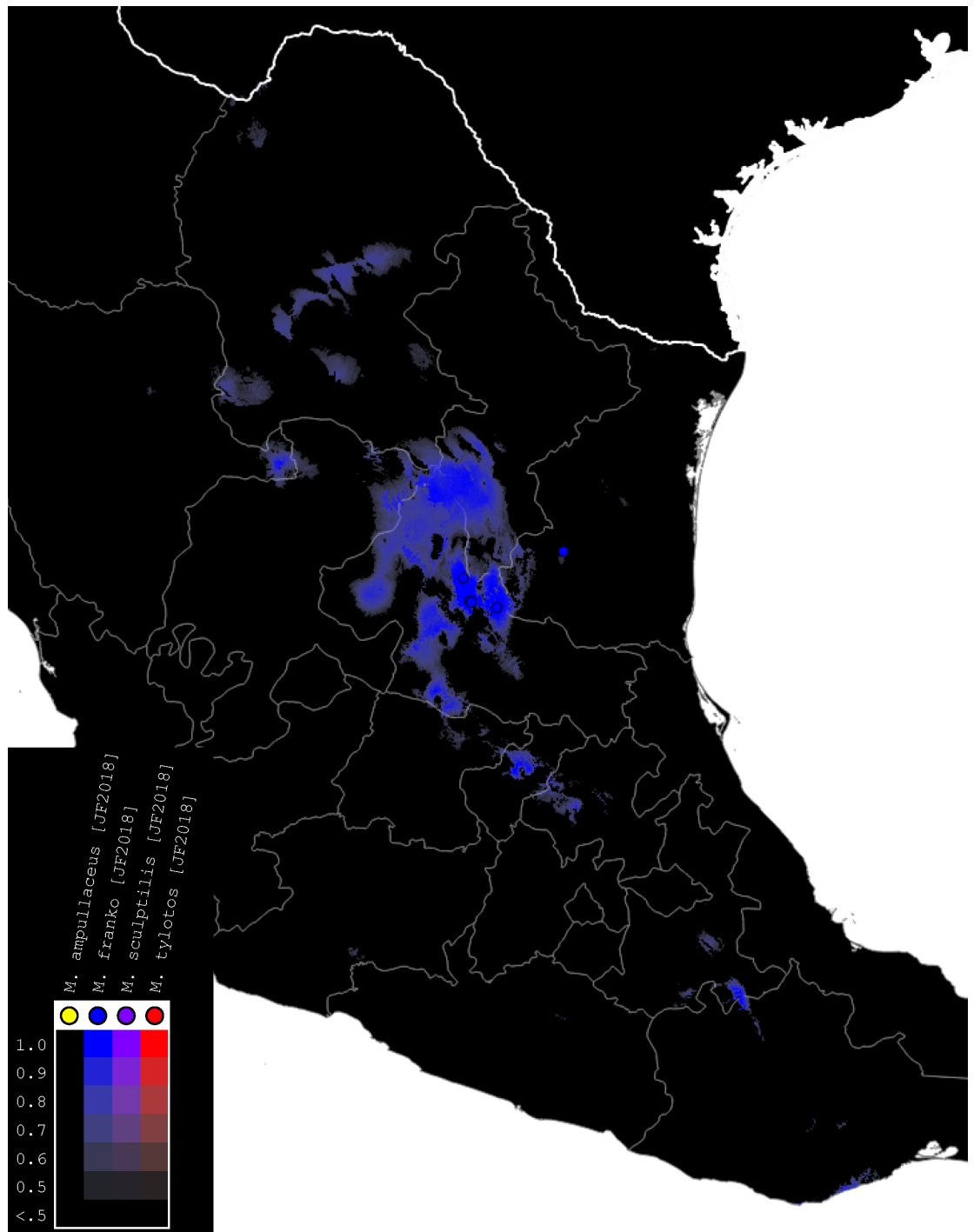


**Figure 37. Distributions of *M. franko* [JF2018].** Combined occurrence record and Maxent habitat modeling map for *M. franko* [JF2018], as indicated in the legend.

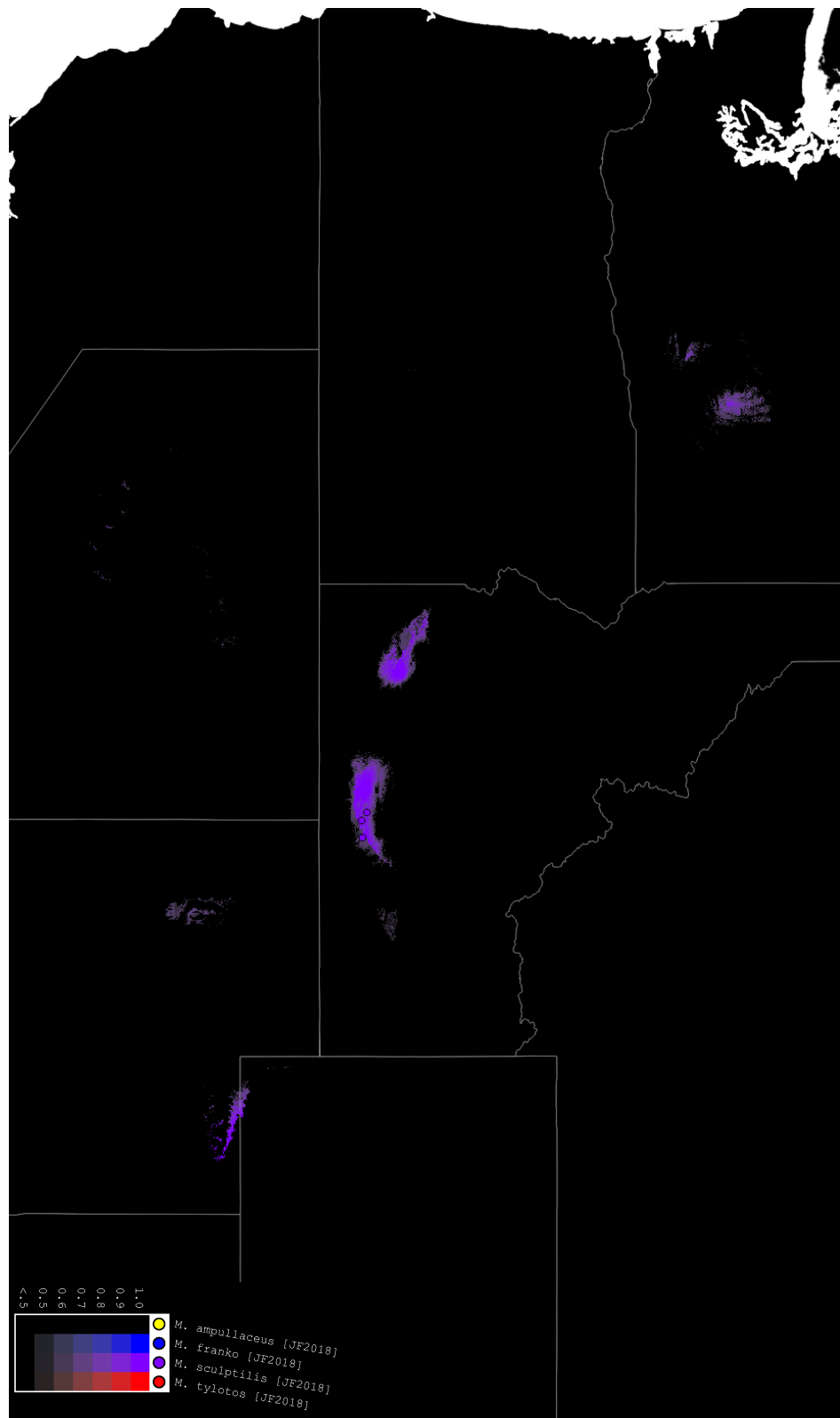


**Figure 38. Distributions of *M. sculptilis* [JF2018].** Combined occurrence record and Maxent habitat modeling map for *M. sculptilis* [JF2018], as indicated in the legend.